Paleomagnetism and rock magnetism from sediments along a continental shelf-to-slope transect in the NW Barents Sea: Implications for geomagnetic and depositional changes during the past 15 thousand years

C. Caricchi[a,*], R.G. Lucchi[b], L. Sagnotti[a], P. Macrì[a], C. Morigi[c,d], R. Melis[e], M. Caffau[b], M. Rebesco[b], T.J.J. Hanebuth[f,g]

[a] Istituto Nazionale di Geofisica e Vulcanologia, Via di Vigna Murata 605, 00143 Rome, Italy
[b] Istituto Nazionale di Oceanografia e di Geofisica Sperimentale (OGS), Borgo Grotta Gigante 42/c, 34010 Sgonico, TS, Italy
[c] GEUS (Stratigraphy Department Geological Survey of Denmark and Greenland), 1350 Copenhagen, Denmark
[d] Dipartimento di Scienze della Terra, Università di Pisa, 56126 Pisa, Italy
[e] Dipartimento di Matematica e Geoscienze, Università di Trieste, 34128 Trieste, Italy
[f] MARUM – Center for Marine Environmental Sciences, University of Bremen, 28359 Bremen, Germany
[g] Department of Coastal and Marine Systems Science, Coastal Carolina University, Conway, SC 29526, USA

ARTICLE INFO

ABSTRACT

Paleomagnetic and rock magnetic data were measured on glaciomarine silty-clay successions along an E-W sediment-core transect across the continental shelf and slope of the Kveithola paleo-ice stream system (south of Svalbard, north-western Barents Sea), representing a stratigraphic interval spanning the last deglaciation and the Holocene.

The records indicate that magnetite is the main magnetic mineral and that magnetic minerals are distinctly less abundant on the shelf than at the continental slope. The paleomagnetic properties allow for the reconstruction of a well-defined characteristic remanent magnetization (ChRM) throughout the sedimentary successions. The stratigraphic trends of rock magnetic and paleomagnetic parameters are used for a shelf-slope core correlation and sediment facies analysis is applied for depositional processes reconstruction. The new paleomagnetic records compare to the PSV and RPI variation predicted for the core sites by a simulation using the global geomagnetic field variation models SHA.DIF.14k and CALS7K.2 and closest PSV and RPI regional stack curves. The elaborated dataset, corroborated by available ^{14}C ages, provides a fundamental chronological framework to constrain the coupling of shelf-slope sedimentary processes and environmental changes in the NW Barents Sea region during and after deglaciation.

1. Introduction

Rock magnetic analyses are known to be a very powerful tool for sedimentary reconstructions of changes in sediment provenance, patterns and strength of oceanic currents and diagenetic effects linked to paleoenvironmental changes (Kissel et al., 1997, 1999; Brachfeld, 2006; Brachfeld et al., 2009, among others). The stratigraphic trends indicated by rock magnetic parameters depend on the environmental variability and can be used for correlating between different depositional settings. In particular, stratigraphic trends in grain size, as well as concentration and type of magnetic minerals provide valuable information on changes in the environmental conditions that have an effect on the geochemical composition of pore water and sediments (e.g., Snowball and Torii, 1999; Sagnotti et al., 2001; Larrasoaña et al., 2003, 2007; Brachfeld et al., 2009). Moreover, concentration, composition, and grain size of the magnetic minerals contain evidence for sediment source, sediment transport processes, and marine productivity (Robinson, 1986; Kissel et al., 1997, 1999, 2003; Stoner and Andrews, 1999; Brachfeld et al., 2002, 2013; Muhs et al., 2003; Hounslow and Morton, 2004; Rousse et al., 2006). As observed by several studies, changes in rock magnetic stratigraphic trends coincide with climatic changes during glacial and interglacial phases (Dearing, 1999; Liu et al., 2012 and reference therein). The concentration of magnetic minerals may reflect dilution effect due to the presence of biogenic carbonate and silica, and of organic matter (Thompson and Berglund, 1976; Thompson et al., 1985; Zolitschka and Negendank, 1996;

Dearing, 1999), but it is also primarily controlled by dissolution of ferromagnetic minerals under anoxic conditions, where these minerals (as magnetite) become thermodynamically instable (Leslie et al., 1990; Nowaczyk et al., 2000; Roberts, 2015).

Moreover, paleomagnetic data sets allow for the reconstruction of geomagnetic field paleosecular variations (PSV) and relative paleointensity (RPI) trends, which in turn are useful to define high-resolution age models for sedimentary successions.

Previous studies proposed regional reference records based on both stacked PSV curves (Turner and Thompson, 1981, 1982; Hagstrum and Champion, 2002) and global geomagnetic field models (Korte and Constable, 2005; Korte et al., 2005, 2009; Donadini et al., 2009; Pavón-Carrasco et al., 2014), mainly based on paleomagnetic and archeomagnetic data from low and mid-latitudes. In the last few years, some authors proposed paleosecular variation records measured in sedimentary cores at high latitudes highlighting the pivotal importance of these geomagnetic field variation reconstructions to define and refine geomagnetic field models (Haltia-Hovi et al., 2010; Sagnotti et al., 2011; Stoner et al., 2013; Lougheed et al., 2014).

The paleomagnetic and rock magnetic characteristics of the sedimentary succession forming the Storfjorden-Kveithola Trough Mouth Fan (TMF) system, located in the North-western Barents Sea continental margin, south of Svalbard (Fig. 1), has been studied in the framework of the SVAIS (Spanish IPY activity; https://sites.google.com/site/ipynicestreams/svais) and OGS-EGLACOM (Italian contribution to IPY; https://sites.google.com/site/ipynicestreams/eglacom Italian contribution to IPY) projects (Sagnotti et al., 2011, 2016). TMFs are cone-like bathymetric features located on the continental slope area that originated by the pile-up of detritic sediments delivered by fast-flowing ice (ice streams) during shelf-edge glaciations, and pelagic deposition occurring during interglacial stages. Therefore, TMFs contain the record of past climatic changes, and represent suitable areas for reconstruction of paleoclimatic, paleoceanographic, and paleoglacial history of polar continental margins (Alley et al., 1989; Vorren et al., 1989, 1998; Vorren and Laberg, 1997; Laberg et al., 2005; Dowdeswell et al., 2008, among others). At the same time, the study of the

sedimentary record contained in glacial troughs, formed by basal erosion of the former ice streams advancing during glacial maxima, can give information on the modality of the ice sheet retreat and related sea level rise during deglaciation especially during their latest phases when sediment meltwater deposition was confined to the shelf area (Lucchi et al., 2013). Indeed shelf and slope areas contain complementary paleo-depositional information the merge of which would allow a more reliable reconstruction of the Svalbard-Barents Sea Ice Sheet history after Last Glacial Maximum (LGM).

Although previous studies attempted to correlate shelf and slope cores on the basis of sediment magnetic susceptibility and radiocarbon dating (e.g., Jessen et al., 2010), this region still lacks a proper paleomagnetic stratigraphy and rock magnetic characterization that allow for establishing a reliable and original framework for along- and across-slope core-correlation purposes. To fill this gap, the present study, conducted within the Italian PNRA project CORIBAR-IT, aims at correlating the sedimentary successions, collected along an E-W-oriented transect of sediment cores across the slope and shelf of the Kveithola glacigenic system, through paleomagnetic and rock magnetic analyses. The Storfjorden-Kveithola glacial depositional system was chosen as study area because sustained by a relatively small ice catchment area (Elverhøi et al., 1995; Mangerud et al., 1998). The short distance (some kilometers only) from the source of ice to the calving areas resulted in a rapid response to climatic changes. In this work, we compare our data with the recent stacked PSV curves and with geomagnetic field variations extrapolated by global and regional (mid-latitude) PSV models adding a piece of knowledge about geomagnetic field variations at high latitude during the last 15 ka.

2. Geomorphological setting and climate-related depositional processes

The Kveithola glacigenic system is located in the Northwestern Barents Sea, south of the Svalbard archipelago (Fig. 1). The Kveithola Trough hosted ice-streams during last glaciation (Marine Isotope Stage/MIS-2) that reached the shelf edge during the Last Glacial Maximum
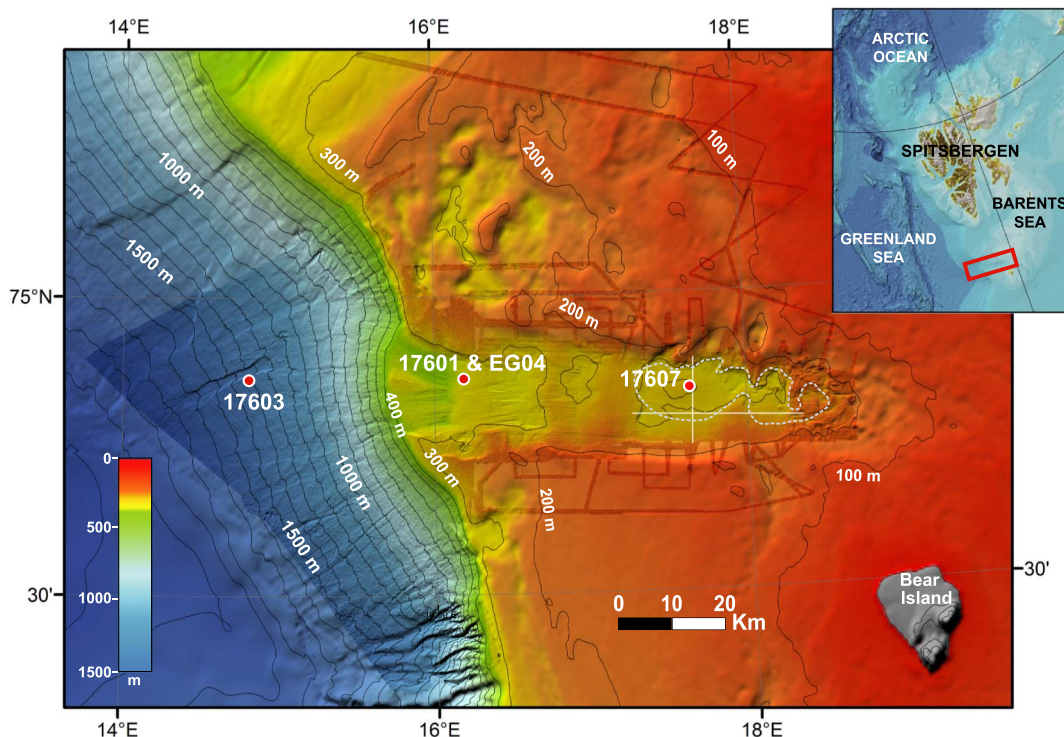

Fig. 1. Bathymetric map of the Kveithola glacigenic trough with location of the discussed CORIBAR and EGLACOM cores.

(LGM) (Pedrosa et al., 2011; Rebesco et al., 2011; Rüther et al., 2012; Bjarnadóttir et al., 2013). The E-W trough is relatively small with a length of 90 km from the shelf edge to the eastwards termination, and < 15 km wide. The water depth inside the trough deepens from 200 to 400 m, and the U-shaped cross-section has steep flanks, dipping by about 2° (Rüther et al., 2012). The almost flat trough axis gently dips toward the shelf edge with a stair-like topography produced by a series of transversal sediment ridges. According to Rebesco et al. (2011) these ridges are grounding-zone wedges (GZWs) derived by deposition of unconsolidated, saturated subglacial till during episodic stillstands of the overall ice-stream retreat during last deglaciation. The inner area of the trough contains a complex sediment drift composed by two depocenters (Main and Minor drifts, Rebesco et al., 2016) whose onset was related to the interplay of Atlantic and Arctic waters (West and East Spitzbergen currents respectively), and brine-enriched shelf water (BSW, Aagaard et al., 1985; Fohrmann et al., 1998; Thomsen et al., 2001) produced on the shelf during winter which formation started at around 13 cal ka BP (Rebesco et al., 2016).

The Kveithola TMF merges with the neighboring, larger Storfjorden TMF, together forming the Kveithola-Storfjorden TMF system built by glacigenic deposits during full glacial conditions and glacimarine sediments during interglacials (Vorren and Laberg, 1997; Lucchi et al., 2013). Glacial deposits in this area consists of high-density glacigenic diamicton, usually found in the upper part of the slope, providing evidence of shelf edge glaciation during Last Glacial Maximum (LGM), and low-density glacial debrites that testify slope instability of the Kveithola TMF during and after the LGM (Lucchi et al., 2013; Llopart et al., 2016). The transition from fully glacial to interglacial conditions (deglaciation) is characterized by massive input of ice rafted debris (IRD) and terrigenous sediments delivered by meltwater, associated with the decay and retreat of the local ice sheet. The deposition during interglacial conditions was of hemipelagic nature with biogenic rich sediments locally reworked by contour currents (Lucchi et al., 2013; Rüther et al., 2012).

3. Material and methods

This study is based on four gravity cores and three box cores recovered along a shelf-to-slope transect in the Kveithola glacial system, which were taken during two oceanographic cruises: the OGS-EGLACOM cruise on board RV OGS-Explora (Kristiansund-Kristiansund, July 8 to August 4, 2008), and the CORIBAR MSM30 cruise with RV Maria S. Merian (Tromsø-Tromsø, July 16 to August 15, 2013; Hanebuth et al., 2013, 2014). The sediment cores where collected from three depositional settings: (i) the contourite drift inside the Kveithola trough (Core GeoB17607-5 and GeoB17607-4); (ii) the outermost Kveithola Trough on a GZW (Cores GeoB17601-3, GeoB17601-2, and EG-04), and (iii) the middle continental slope on the Kveithola TMF (Cores GeoB17603-3 and GeoB17603-2) (Table 1, Fig. 1).

The core sections were x-rayed prior to opening. The open cores were visually described and photographed with a Geotek-MSCL digital camera. The working halves were sampled with u-channel plastic

holders with 2 × 2 cm cross section for continuous paleomagnetic and rock magnetic measurements, and for an element-intensity analysis with an Avaatech XRF (X-ray fluorescence) core scanner using 10 kV for light and 30 kV for heavy element detection. In particular, we considered the content of Calcium (Ca), Iron (Fe), Zircon (Zr), Rubidium (Rb), Bromium (Br), and Clorine (Cl), using the Ca/Fe ration as a proxy for biogenic vs. terrigenous (e.g. Lucchi et al., 2013; Carbonara et al., 2016); the Zr/Rb ratio was used as proxy for coarse sediment distribution (e.g. Wang et al., 2011), as Zr is usually associated with sandy material whereas Rb is enriched in sediment containing clay minerals; and the Br/Cl ratio was used as proxy for organic matter content as the Br is often associated with the organic carbon (e.g. Thomson et al., 2006; Rothwell et al., 2006). Compositional analyses made on smear slides and binocular microscope indicated that the Ca content is primary related to the biogenic fraction. Titanium (Ti) content is widely used as litho-proxy due to its inert/insoluble characteristics. Nevertheless, as in our cores the down-core trends of Ca/Ti and Ca/Fe ratios were identical, we decided to use the latter proxy giving additional, indirect information on Fe distribution useful for the identification of oxidized layers.

Discrete samples from the gravity cores were collected at every 10 cm from Cores EG-04 and 17603-3 for grain-size analysis performed with a Beckman Coulter LS-230 laser particle size analyzer (0.04–2000 μm fraction at 0.004 μm resolution). Samples were treated for 24 h with peroxide to remove the organic matter. The sediment samples were then re-suspended into a 0.1% sodium-hexametaphosphate solution and left for 3 min in ultrasonic bath prior to the analyses.

Sediment samples from the box-cores were collected at every 10 cm depth for the determination of the total organic carbon (Corg) using a NA-2100 Elemental Analyzer, following the procedure described by Nieuwenhuize et al. (1994). The measured total organic carbon was then converted to organic matter (OM) content following Gordon (1970): Table 2.

Nineteen samples from Cores EG04 and 17603-3 were dated by (Accelerator Mass Spectrometry (AMS) ^{14}C dating on planktonic foraminifera tests at National Ocean Sciences Accelerator Mass Spectrometry (NOSAMS) Laboratory (U.S.A.), whereas the base of Core 17607-5, was dated with a scaphopod shell at the Poznan Radiocarbon Laboratory (Poland; cf. Rebesco et al., 2016). The raw ^{14}C data were calibrated with the CALIB software version 7.1 (Stuiver and Reimer, 1993) using the Marine13 calibration curve (Reimer, 2013), and applying an average marine regional reservoir effect ΔR = 67 ± 34 years, obtained from the Marine Reservoir Correction Database of Calib 7.1 for the North-Western Barents Sea area (Mangerud and Gulliksen, 1975). The calibrated ages are provided with their ± 1σ and ± 2σ ranges and reported as cal a BP and cal ka BP (Table 3). The median probability of the probability distribution is used since this value is considered the most probable approximation to a real calendar age (Telford et al., 2004).

Paleomagnetic and rock magnetic measurements were carried out on the CORIBAR cores in a magnetically shielded room in the

Table 1
Location of the CORIBAR and EGLACOM cores.

Core ID[a]	Gear	Latitude (N)	Longitude (E)	Water depth (m)	Location	Recovery (m)
GeoB17601-2	Box core	74° 51,53′	16° 05,82′	384	Outer trough GZW	0.43
GeoB17601-5	Gravity core	74° 51,53′	16° 05,82′	369	Outer trough GZW	5.09
GeoB17603-2	Box core	74° 51,00′	14° 48,09′	1425	Kveithola TMF	0.49
GeoB17603-3	Gravity core	74° 51,00′	14° 48,08′	1431	Kveithola TMF	9.90
GeoB17607-5	Box core	74° 50,74′	17° 38,35′	298	Inner trough main drift	0.34
GeoB17607-5	Gravity core	74° 50,71′	17° 38,28′	298	Inner trough main drift	9.20
EG04	Gravity core	74° 51.89′	16° 05.60′	374	outer trough GZW	1.05

[a] GeoB176xx = CORIBAR cores; EGxx = EGLACOM cores; GZW = grounding zone wedge; TMF = trough mouth fan.

Table 2
Organic carbon (Corg) and Organic Matter (OM) weight%.

Sample ID	cmbsf	Corg(%)	[a]OM (%)
GeoB17601-2	0	0.96	1.73
GeoB17601-2	10	0.86	1.55
GeoB17601-2	20	0.84	1.51
GeoB17601-2	30	1.00	1.80
GeoB17603-2	0	1.14	2.05
GeoB17603-2	10	0.82	1.48
GeoB17603-2	20	1.05	1.89
GeoB17603-2	30	0.70	1.26
GeoB17603-2	40	0.64	1.15
GeoB17607-1	0	2.21	3.98
GeoB17607-1	10	2.15	3.87
GeoB17607-1	20	2.44	4.39
GeoB17607-1	30	2.02	3.64
GeoB17607-1	40	2.03	3.65

[a] OM = Corg × 1.8 (Gordon, 1970).

paleomagnetic laboratory at the Istituto Nazionale di Geofisica e Vulcanologia, Rome. For each u-channel, the natural remanent magnetization (NRM), the low-field magnetic susceptibility (k), and anhysteretic remanent magnetization (ARM) were measured in 1 cm increments. The NRM was measured on a small-access (45 mm diameter) automated pass-through 2G Enterprises DC SQUID 755 superconducting rock magnetometer (SRM), while k was measured using a Bartington magnetic susceptibility meter equipped with a MS2C sensor with an internal diameter of 45 cm and mounted in-line with the SRM translating system. For the NRM measurements, the half-width of the response function of the three orthogonal Superconducting Quantum Interference Device (SQUID) pick-up coils of the SRM system varies between 4.1 and 6.7 cm for the transverse (X and Y axes) and the axial (Z axis) respectively. The spurious effects related to the SQUID response functions were corrected directly by the measuring software, normalizing the magnetic signal recorded by each pick-up coil by the area under the respective response curve and compensating the negative regions on the edge of the SQUID response functions for the X and Y axes and the broader width of the SQUID response function along the Z axis (Roberts, 2006). The computed paleomagnetic data are therefore truly independent every ca. 5 cm and are free from artifacts that may arise from uncompensated raw magnetic moment data (Roberts, 2006). We adopted a conservative approach by disregarding the paleomagnetic data for ~5 cm at both ends of each u-channel and the associated

artificial stratigraphic gap. We also disregarded anomalous paleomagnetic and magnetic values related to disturbed sediments.

As a first step, magnetic susceptibility measurements were performed. Subsequently, the NRM was progressively subjected to alternating field (AF) demagnetization in nine steps up to a maximum peak field of 100 mT (steps: 0, 5, 10, 15, 20, 30, 40, 50, 60, 80, 100 mT). After each NRM demagnetization cycle, an anhysteretic remanent magnetization (ARM) was imparted on each u-channel, using an in–line single axis direct current (DC) coil, coupled with the AF coils. An axial 0.1 mT bias DC field and a symmetric AF peak of 100 mT along the Z axis were applied while the u-channel was translated through the AF and DC coil system at a constant speed of 10 cm/s, being the slowest speed allowed by the software running the measurement. The translation speed has an effect on the efficiency of AF demagnetization and the intensity of the produced ARM (Sagnotti et al., 2003; Brachfeld et al., 2004). The adopted procedure equals an AF decay rate of 67 µT per half-cycle and results in the highest ARM intensity achievable with the employed instrumental setting and management software (Sagnotti et al., 2003). Since both NRM and ARM are almost single component magnetic remanences, the median destructive field (MDF) for each core interval measured was automatically computed from AF demagnetization curves (MDF_{NRM} and MDF_{ARM}, respectively). MDF is defined as the value of peak AF required to reduce the remanence intensity to half of its initial value, and it is a coercivity-dependent magnetic parameter.

The MDF_{NRM} was estimated with Demagnetization Analyses in Excel (DAIE) Software (Sagnotti, 2013) avoiding the bias related to possible presence of multiple not-parallel remanence components. The MDF_{NRM} was computed from a plot using the sum of vector difference magnitudes (VDS) (Gee et al., 1993) between successive demagnetization steps and showing the remanence intensity decay as a percentage of the initial value. The low-field magnetic susceptibility (k) and the ARM intensities mostly depend on the concentration of ferromagnetic (sensu lato) minerals. However, these two concentration-dependent rock magnetic parameters carry different information. The magnetic susceptibility values are determined by the contribution of all the rock-forming minerals, in proportion to their relative abundance and specific magnetic susceptibility. The ARM is primarily sensitive to the concentration of fine, single-domain (SD), ferrimagnetic grains (King et al., 1982; Maher, 1988). The ARM/k ratio was computed in order to define trends in ferrimagnetic grain size, since high ratios are related to single domains grains, while low values indicate a predominance of multi-domains grains (Banerjee et al., 1981). Finally, the ΔGRM/ΔNRM ratio

Table 3
Accelerator Mass Spectrometry (AMS) ^{14}C dating. Sample ID report indication of sample depth.

Lab ID	Sample ID	Type	Age	Age err	cal yr BP 1sigma	cal yr BP 2sigma	Median probability cal yr BP
OS-123791	17603-3-0[a]	*N. pachyderma* sin	720	20	257–336/344–356	151–159/227–424	302
OS-123794	17603-3-10	*N. pachyderma* sin	1260	30	680–775	653–854	736
OS-123804	17603-3-20[a]	*N. pachyderma* sin	2280	35	1745–1873	1686–1938	1813
OS-123422	17603-3-30	*N. pachyderma* sin	2580	45	2118–2274	2028–2317	2183
OS-123805	17603-3-50	*N. pachyderma* sin	3560	35	3323–3440	3236–3502	3377
OS-123796	17603-3-80[a]	*N. pachyderma* sin	4590	35	4654–4663/4673–4807	4569–4832	4723
OS-123408	17603-3-140[a]	*N. pachyderma* sin	6520	50	6851–7027	6787–7129	6946
OS-123536	17603-3-160[a]	*N. pachyderma* sin	6840	35	7250–7357	7201–7408	7303
OS-123786	17603-3-210[a]	Mix planktic	7750	40	8054–8200	8010–8281	8143
OS-123404	17603-3-240	*N. pachyderma* sin	8240	65	8544–8777	8479–8933	8676
OS-123406	17603-3-270	*N. pachyderma* sin	8440	60	8848–9069	8706–9171	8954
OS-123409	17603-3-360[a]	Mix planktic	8770	60	9299–9450	9199–9509	9370
OS-123657	17603-3-660[a]	*N. pachyderma* sin	10,900	40	12,221–12,476	12,085–12,539	12,335
OS-123405	17603-3-680	*N. pachyderma* sin	11,650	80	12,951–13,169	12,834–13,263	13,059
OS-123411	17603-3-820[a]	Mix planktic	12,400	120	13,652–13,957	13,495–14,083	13,800
OS-123425	1760-3-970	Mix planktic	12,850	170	14,126–14,802	13,957–15,125	14,505
Poz-63467	17607-5-920[b]	Scaphopods	9250	50	9891–10,107	9754–10,160	9980
OS-97979	EG04-4	Foraminifera	680	20	225–305	129–362	259
OS-78386	EG04-90	Foraminifera	12,000	280	13,123–13,711	12,799–13,992	13,799

[a] After Carbonara et al., 2016.
[b] After Rebesco et al., 2016.

provides a quantitative measure of the tendency to acquire a spurious gyromagnetic remanent magnetization (GRM) at high AF steps, and is a proxy for the occurrence of iron sulphides, especially greigite (Fu et al., 2008). ΔGRM represents the difference between the final remanence intensity measured at the last applied AF step and the intensity minimum value (MV) measured during the whole AF treatment. ΔNRM represents the difference between the initial remanence intensity value and MV.

4. Results

4.1. AMS ^{14}C dating

AMS ^{14}C dating on the Kveithola TMF (Core 17603-3) were performed in correspondence of characteristic peaks of the magnetic susceptibility recognizable in most of the cores studied in the southern and western margin of Svalbard (Jessen et al., 2010; Lucchi et al., 2013; Carbonara et al., 2016). The calibrated ages indicate that Core 17603-3 contains the post LGM depositional sequence starting from about 15 cal ka BP (Table 3). Dating of the shelf cores indicates the presence of a condensed stratigraphic sequence on the outer shelf area compared to both the slope core and inner shelf area where over 9 m of sediments deposited during about 10 ka (Core 17607-5, Table 3).

4.2. Sediment facies analyses

The studied cores contain five main sedimentary facies (Fig. 2) from which we determined specific depositional processes on the basis of

visual descriptions of the sediments, textural and compositional analyses, also taking into account the facies analyses made by Lucchi et al. (2013) and Rüther et al. (2012) in this area.

4.2.1. Interlaminated facies

This facies consists of finely laminated gray mud interbedded with dark gray silt laminae and layers. This facies was previously interpreted as resulting from sediment-laden meltwater plumes produced by the ice-stream melting (Lucchi et al., 2013). The interlaminated facies is found at the bottom of the slope in Core 17603-3 and in the outer-shelf Core 17601-3.

4.2.2. IRD-rich facies

IRD grain and pebbles occurs in massive cm-thick discrete layers, and sparsely distributed within the bulk sediments. In the latter case, the sediments are predominantly terrigenous and bioturbated, although they can contain bioclasts like foraminifera, bivalves and scaphopods on the shelf area. The IRD massive facies was observed in Cores 17603-3 (slope) and 17601-3 (outer trough) overlying the interlaminated sediments and overlaid by the sparsely distributed IRD facies. In agreement with the previous facies interpretation, the massive facies is associated with high iceberg calving rates and/or collapse of the ice stream (Lucchi et al., 2015), whereas the scattered presence of IRD in bioturbated sediments suggests low iceberg calving rates in progressively distal glacimarine conditions (grain size fining up-core, Fig. 2).

4.2.3. Crudely layered facies

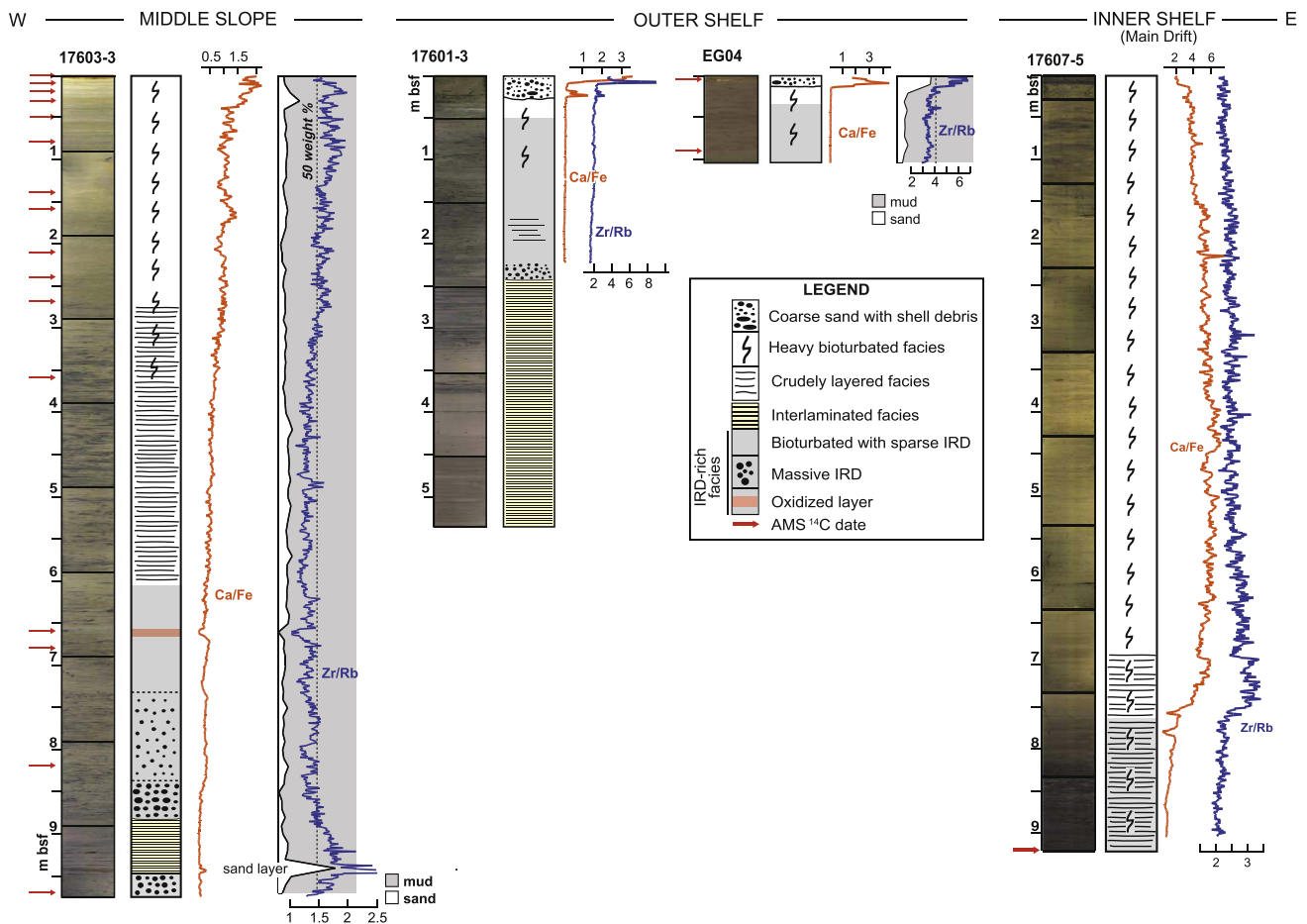Fine-grained, diatom-bearing sediment with coarse bedding, was

Fig. 2. Core photographs and lithological logs with compositional and textural proxies. Ca/Fe ratio tracks biogenic vs. terrigenous input, whereas the Zr/Rb ratio is a proxy of coarse sediment distribution. The sand/mud down-core distribution obtained on individual samples is also reported in comparison with the Zr/Rb ratio. mbsf = meters below sea floor.

mainly observed on the slope Core 17603-3, although some crude bedding was observed also in the terrigenous sediments of the outer trough in Core 17601-3, above the massive IRD facies, and at the base of the inner trough Core 17607-5. In the shelf cores, this facies contains a higher percentage of terrigenous sediment including IRD, and macro-benthic fauna (bivalve and scaphopods) that are absent in the slope core. Crude sediment bedding with multimodal grain size spectra was associated with the deposition under bottom currents coherently with the interpretation made by Lucchi et al. (2013).

4.2.4. Heavily bioturbated facies

This facies consists of pervasively bioturbated sediment with a fine-grained texture at the slope (mean average grain size 7.12 phi, i.e., medium silt) and a coarser texture on the shelf (mean average grain size 6.20 phi, i.e., coarse silt). This facies is particularly developed in the slope Core 17603-3 and the shelf Core 17607-5 from the inner Kveithola trough Main Drift. The sediments recovered from the slope contain a relatively higher percentage of terrigenous components with respect to the shelf area, as also depicted by the Ca/Fe ratio. The biogenic fraction on the shelf comprises benthic macrofauna (e.g. bivalve and scaphopods), whereas the detritic component includes sparse IRD particles, which are virtually absent on the slope. The sediments recovered from the Main Drift (Core 17607-5) are generally characterized by a considerably higher content of organic matter with respect to the outer shelf and the slope area (Table 2, Fig. 3). The sedimentological and compositional characteristics of the heavily bioturbated facies suggest the deposition occurred by hemipelagic settling under bottom currents influence.

4.2.5. Coarse sand with shell debris

The sedimentary sequence in the outer trough is topped by a cm-thick (20 cm thick in Core 17601-3) interval of sandy silt (mean average grain size 5.22 phi, i.e., very coarse silt) containing abundant shell debris. The contact with the underlying sediments is sharp and locally irregular. This stratigraphic contact corresponds to a sharp

Fig. 3. Down-core variation of Br/Cl ratio within core17601-3 (blue), 17603-3 (red) and 17607-5 (green) used as proxy of Organic Matter content in the sediments with high Br/Cl ratio corresponding to high Organic Matter content. The inner Kveithola Trough (Core 17607-5) is characterized by higher organic matter content with respect to the outer shelf area (Core 17601-3). (For interpretation of the references to colour in this figure legend, the reader is referred to the web version of this article.)

textural and compositional change from fine-grained mainly terrigenous sediments (low Zr/Rb and Ca/Fe ratios, Fig. 2) to coarse-grained sediments rich in bioclasts (high Zr/Rb and Ca/Fe ratios).

4.2.6. Grain size and Zr/Rb ratio

Following Wang et al. (2011), we compared the measured sediment grain size with the Zr/Rb down-core ratio. Although the different sampling resolution (10 cm for the traditional method, and 1 cm for the XRF core scans), the Zr/Rb trend nicely mimics the down-core distribution of sand in Cores 17603-3 and EG04 and, therefore, we used it as proxy for the sediment texture in this shelf-slope sedimentation system (Fig. 2).

4.3. Rock magnetism

The k values of the core from the drift inside the trough (17607-5) are very low and fluctuate between −16 and 16 ($\times 10^{-5}$ SI) (Fig. 4). We point out however that the very low negative values are artifacts. In fact, the k values measured on u-channels with the MS2C probe need to be multiplied for an appropriate correction factor (Bartington Instruments Ltd., 2002; Sagnotti et al., 2003). The applied correction factor ($\times 4$) works well for positive values, but it provides unrealistic low values when applied to negative k values. Anyway, low and negative values in magnetic susceptibility correlate with the abundance of diamagnetic minerals (e.g. Quartz, Calcite, Aragonite, whose magnetic susceptibility ranges between −1.3 and −1.9 $\times 10^{-06}$ SI; e.g., Sagnotti, 2011) in the lithic fraction. In Core 17607-5, the k values are positive in the lower interval, below 7.3 mbsf and they markedly decrease upward. The sharp shift to very low k values corresponds to an increase of Ca/Fe ratio (Fig. 2). These data indicate that ferromagnetic and paramagnetic minerals are present in very low concentration, or they are even virtually absent, in the upper 730 cm of the core. This may be due to a drastic reduction in the detrital input (with almost no paramagnetic clays), an increase in the biogenic fraction and dissolution of ferromagnetic minerals due to diagenetic effects. In fact, the drift area sediments are black, very rich in organic matter (see the above sediment facies description), smell of hydrogen sulfide, and contain benthic fauna assemblages indicating low-oxygen, possibly reducing environmental conditions (Hanebuth et al., 2013). Therefore, the low concentration in ferromagnetic minerals at this site is most likely due to diagenetic dissolution processes. The ARM, MDF$_{NRM}$ and ΔGRM/ΔNRM parameters show the same stratigraphic trend of k, with a marked decrease around the same level (7.3 mbsf) in correspondence of the beginning of finely bioturbated terrigenous silt deposits. The ARM/k is deeply affected by the low k values and provides a not-significant trend (Fig. 4). An apparent increase in MDF$_{NRM}$ is also observed at the core top (53 mT at < 1 mbsf), but this is most likely due to a poor paleomagnetic behavior of the sediment in this portion of the core (see next paragraph). Finally, the crudely layer facies (depth > 7.3 mbsf) is also characterized by a distinct increase of ΔGRM/ΔNRM suggesting the possible occurrence of SD ferrimagnetic iron sulphides (e.g. greigite; Fu et al., 2008) which may grow, and acquire a magnetic remanence, during late diagenesis. For this reason, we prefer to not take into account this portion of the core for the further paleomagnetic analyses.

In the GZW area (Core 17601-3), k values range around an average value of 22 $\times 10^{-5}$ SI (Fig. 5). The ARM, ARM/k and MDF$_{NRM}$ parameters increase toward the top and in particular a marked step occurred around 3.5 mbsf (yellow rectangle), especially for the MDF$_{NRM}$ and it appears linked to a facies variation, where the interlaminated facies passes upward to crudely stratified layers, indicating an environmental change in the depositional system. In detail, the lowermost interval corresponds to plumites deposited during the Meltwater Pulse 1a event. This interval passes toward the top to crudely stratified layers deposited under the action of bottom currents. The MDF$_{NRM}$ stratigraphic trend shows little fluctuations around a mean value of about 20 mT in interlaminated facies deposits whereas it sharply increase up to 40 mT for
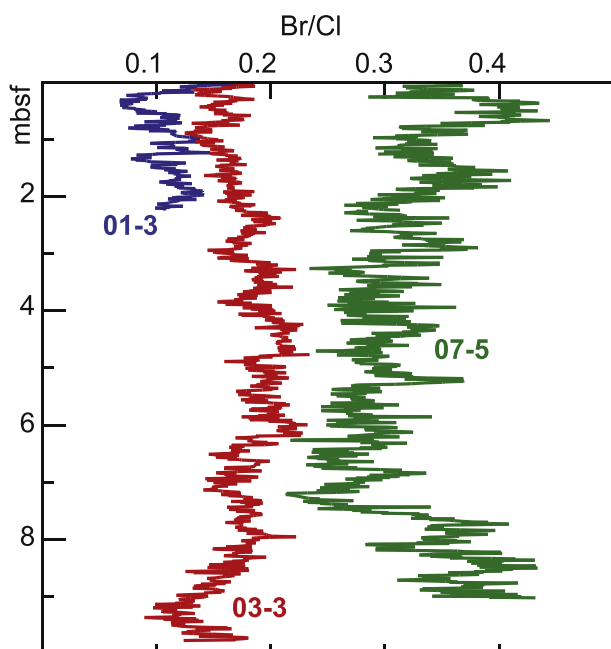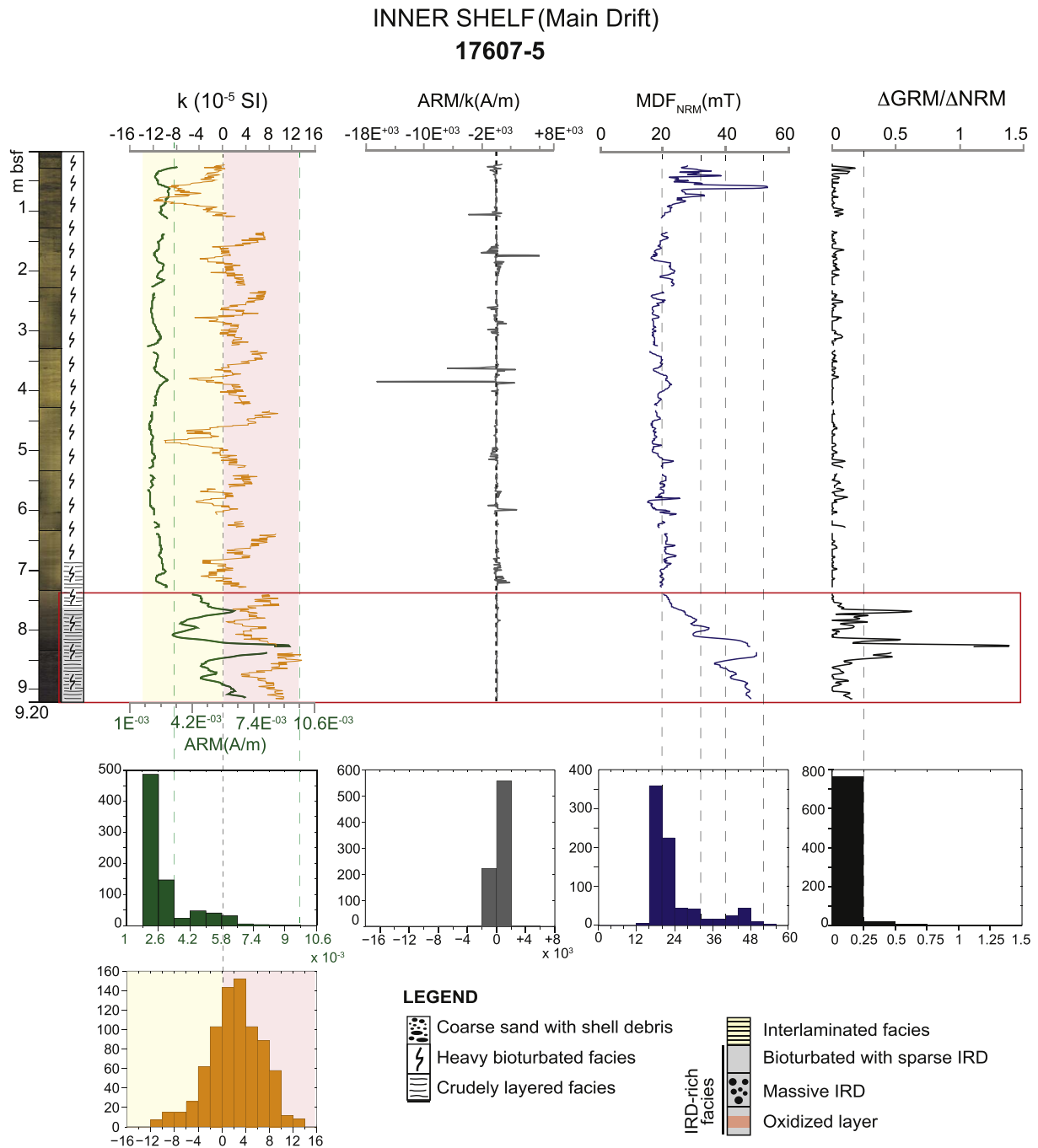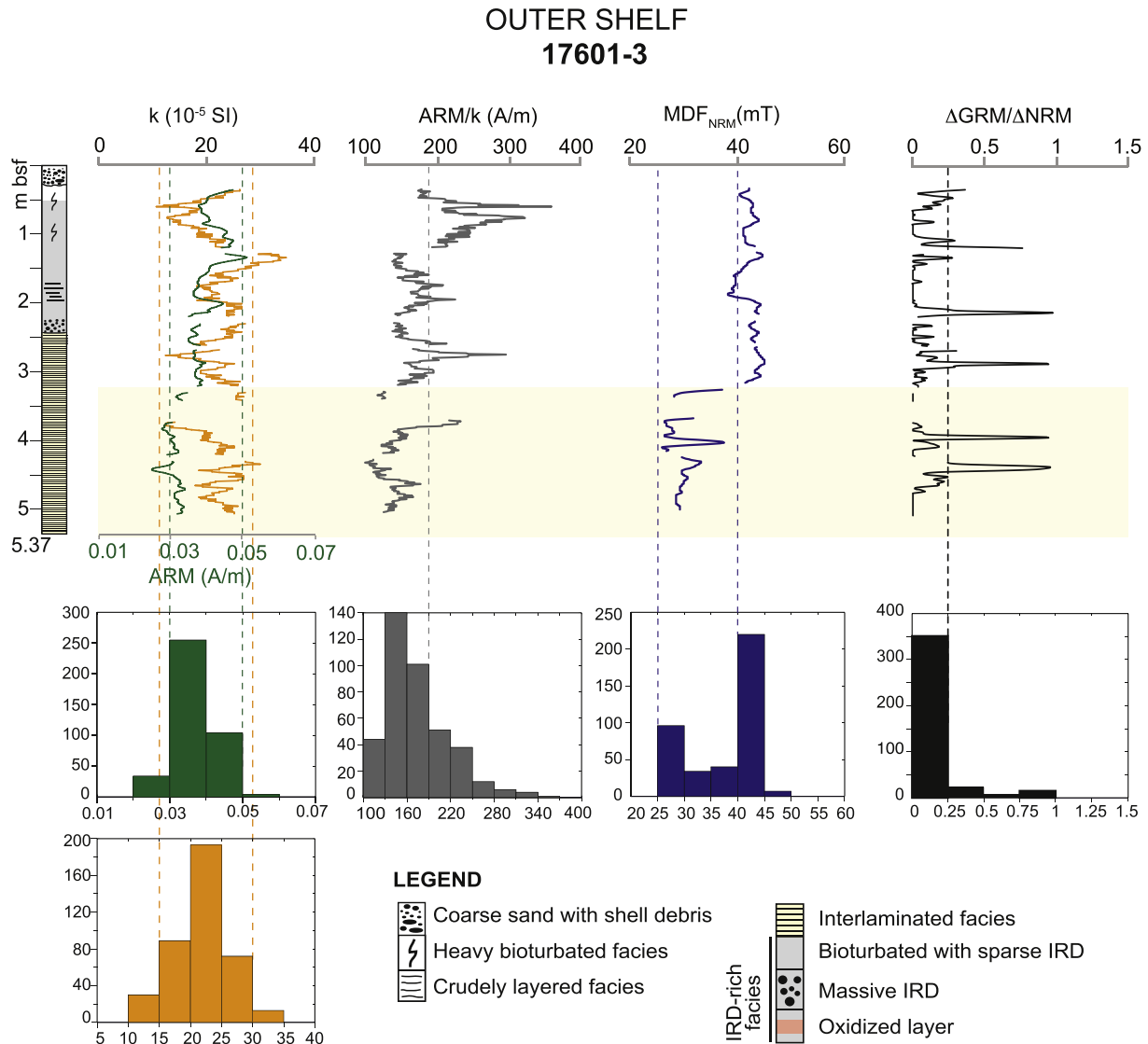
Fig. 4. Stratigraphic trends of the rock magnetic parameters for inner shelf Core 17607-5. The plots show the stratigraphic trend of the intensity of the ARM, the magnetic susceptibility (k), the ARM/k ratio, the MDF$_{NRM}$ and ΔGRN/ΔNRM. A histogram representing the distribution for each parameter has been reported below each graph. The red rectangle indicates an interval (depth > 7.3 mbsf) characterized by an increase in magnetic mineral concentration and coercivity. (For interpretation of the references to colour in this figure legend, the reader is referred to the web version of this article.)

the uppermost part. The observed trend indicates that low-coercivity (multidomain?) grains prevail in the lower part, whereas in the upper part the MDF$_{NRM}$ values vary in the range typical for pseudo-single domain to single-domain magnetite (Maher, 1988). Few discrete levels of GRM acquisition have been observed throughout the core.

The highest k values are recorded in the slope area (17603-3) where k values range around a mean value of 70×10^{-5} SI (Fig. 6). The ARM and ARM/k values increase toward the top, indicating and increase in magnetic minerals concentration and a decrease of coarse-grained fer-rimagnetic minerals, respectively. The MDF$_{NRM}$ is remarkably constant throughout the whole core with a mean value of 29 mT. According to

Maher (1988), the observed range in MDF$_{NRM}$ values is typical for magnetite grains of different size and domain state. The acquisition of spurious GRM at high AF steps is absent. Moreover in correspondence of oxidized layers, peaks of rock magnetic parameters have been observed. Overall, the rock magnetic data collected from the three cores along an E-W transect point out a distinct increase in the concentration of magnetic minerals moving from the inner shelf to the continental slope, as a result of varying depositional settings and diagenetic effects.

Fig. 5. Stratigraphic trends of the rock magnetic parameters for outer shelf Core 17601-3. The plots show the stratigraphic trend of the intensity of the ARM, the magnetic susceptibility (k), the ARM/k ratio, the MDF$_{NRM}$ and ΔGRN/ΔNRM. A histogram representing the distribution for each parameter has been reported below each graph.

4.4. Paleomagnetism

The stepwise demagnetization data were visualized and analyzed with the DAIE software (Sagnotti, 2013). Despite the significant changes in the concentration of magnetic minerals between the cores along the shelf-to-slop transect, the sediment cores are generally characterized by well-defined paleomagnetic properties throughout the sampled stratigraphic intervals, with the exception of uppermost (1 mbsf) and lowermost portions (depth > 7.3 mbsf) of Core 17607-5.

Each stratigraphic section displays a single-component NRM, after removal of a low coercivity viscous remanence at AF peaks of 0–10 mT (Fig. 7). Afterwards, the paleomagnetic directions remain stable up to: i) 40 mT in Core 17607-5; ii) 60 mT in Core 17601-3 and iii) 60–80 mT in Core 17603-3. A well-defined characteristic remanent magnetization (ChRM) was isolated for each measurement interval and its direction was computed by principal component analysis (Kirschvink, 1980) for the demagnetization steps ranging between 15 and 40 mT for Core 17607-5, 15–60 mT for Core 17601-3 and 15–80 mT for Core 17603-3.

The maximum angular deviation (MAD) was computed for each ChRM direction. For the sediment section from the drift area (Core 17607-5), the MAD values are generally higher, but still below 10°, with

the exception of the uppermost 50 cm composed of heavily bioturbated sediment in which MAD values reach a maximum of about 25°. This interval of increased MAD values is also characterized by very low NRM and ARM intensity values and by poorly defined demagnetization diagrams. The MAD is generally lower than 6° for the two more external Cores 17601-3 and 17603-3 (Fig. 8).

The ChRM inclination recorded by Core 17607-5 oscillates around 82° with the exception of lowermost 2 m and the uppermost 1 m, where inclination is much shallower. In Core 17601-3 the ChRM inclination mean value is around 80° for most of the core, although in interlaminated facies distinctly shallower values (down to 41.5°) are recorded. The ChRM inclination trend, observed in Core 17603-3, oscillates around 78°. Both Cores 17601-3 and 17603-3 show a slightly lower ChRM inclination than the expected inclination value of 82.4° for a geomagnetic axial dipole field at 75° N latitude (Fig. 8). As the cores were not azimuthally oriented the ChRM declination of each u-channel was arbitrarily oriented. Therefore, the mean declination value of each u-channel was considered as rotation angle and had been subtracted (or added) to each measured declination value in an attempt to line-up the declination trend for the whole core with the true north. The results are shown in Fig. 8.
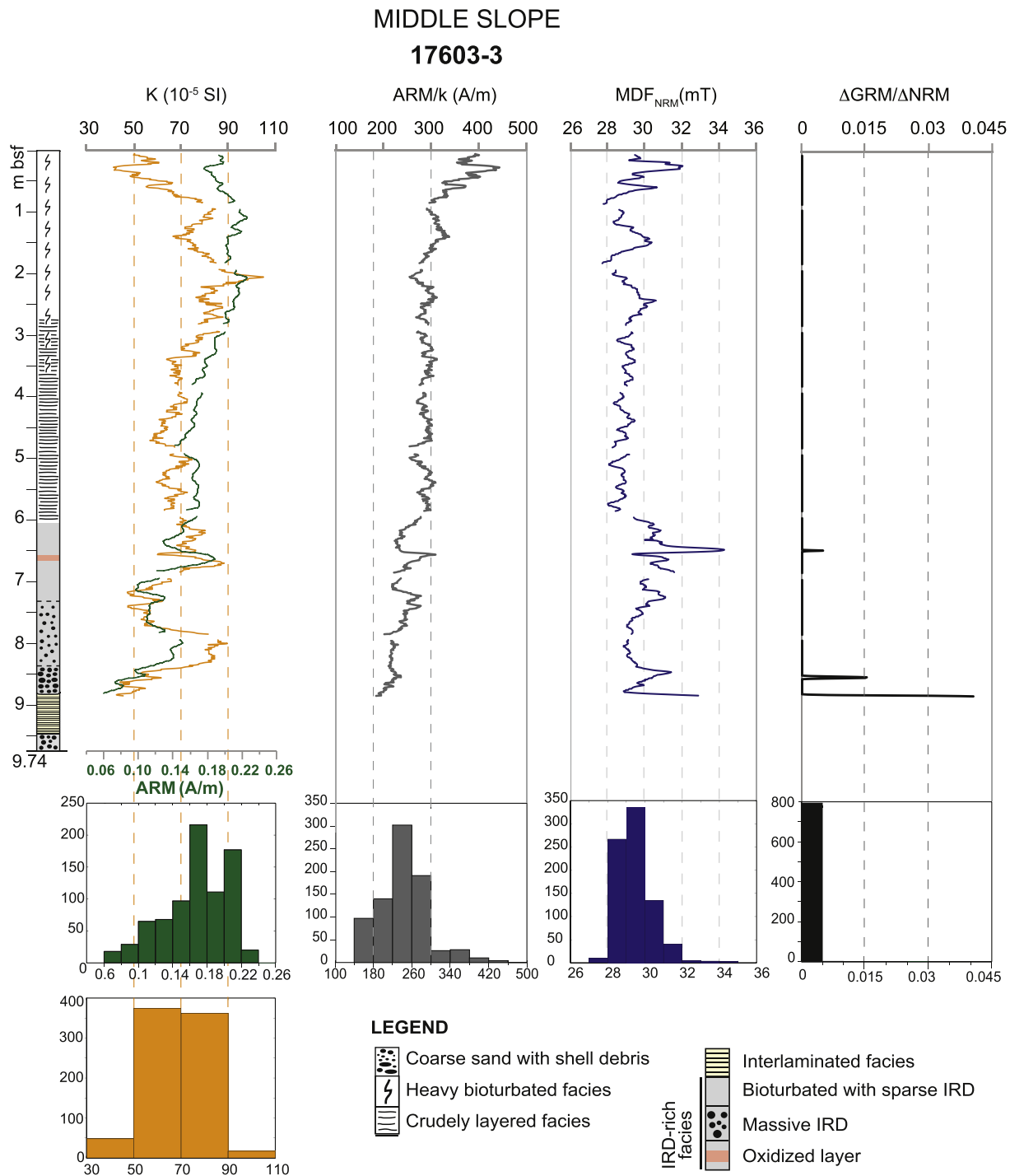
Fig. 6. Stratigraphic trends of the rock magnetic parameters for slope Core 17601-3. The plots show the stratigraphic trend of the intensity of the ARM, the magnetic susceptibility (k), the ARM/k ratio, the MDF$_{NRM}$ and ΔGRN/ΔNRM. A histogram representing the distribution for each parameter has been reported below each graph.

The NRM intensity reflects the geomagnetic field strength during the remanence acquisition time but is also dependent up on the concentration of the NRM-carrying minerals in the sediment.

As for the k and ARM values, the NRM values also increase along the transect from shelf to the slope. The lowest values were recorded in Core 17607-5 and a sharp decrease occurs at 7.3 mbsf in correspondence of the marked change in the rock magnetic parameters. In Core 17601-3 an increase have been observed in correspondence of the facies change around 3.5 mbsf, while in Core 17603-3 the NRM trend oscillate around a mean value 5.60×10^{-2} with exception of the depth >

6.8 mbsf (purple rectangle in Fig. 8) where lower values have been observed in correspondence of the IRD-rich facies.

Relative paleointensity (RPI) curves have been computed by normalizing the NRM intensity opportune with a concentration-dependent rock magnetic parameter (King et al., 1983; Tauxe, 1993). In particular, the NRM remaining after demagnetization in 20 mT AF (NRM$_{20mT}$) was normalized by using both magnetic susceptibility (k) and the ARM intensity left after demagnetization in 20 mT AF (ARM$_{20mT}$) (Fig. 9). In the case of Core 17607-5, the RPI curve was reconstructed by using only the NRM$_{20mT}$/ARM$_{20mT}$ ratio because the low values of k hindered
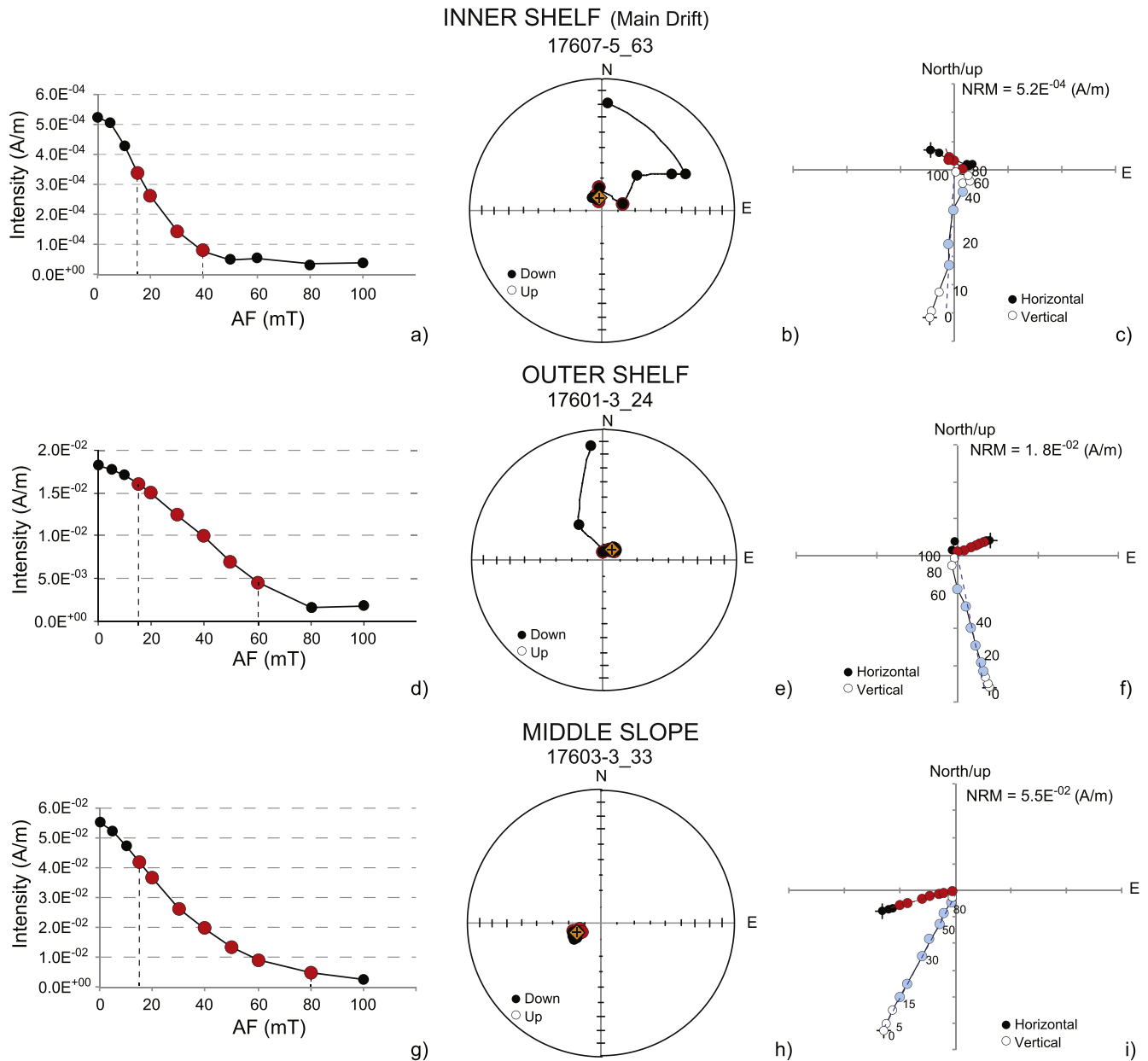
Fig. 7. Representative NRM AF demagnetization graphs for intervals. The demagnetization data have been visualized and analyzed using the DAIE program (Sagnotti, 2013). From left to right: a) d) g) variations of the NRM intensity as a function of the demagnetization steps; b) e) h) Stereographic (equal area) projection of unit vectors defined at each demagnetization steps; c) f) i) Orthogonal projection diagrams of vector measured at each demagnetization step with projection on the North-South vertical plane.

normalization. For the other two cores, both methods generate the similar RPI patterns, indicating a substantial coherency between the two normalization methods.

5. Discussion

5.1. Core-correlations

One of the main purposes of this study is the high-resolution correlation between the Kveithola trough (shelf) and TMF (slope) sedimentary successions on the basis of paleomagnetic and rock magnetic parameters. The stratigraphic trends of rock magnetic and paleomagnetic parameters of Cores 17601-3 and 17607-5 were correlated with those of Core 17603-3, using a sufficient number of calibrated radiocarbon ages. The existing ^{14}C ages in Core EG04 were used as check points to corroborate the final age model as Core EG04 constrains the

sedimentary succession recovered at site 17601-3. The correlations have been carried out by an original software consisting in a single Microsoft Excel workbook (Sagnotti and Caricchi, in preparation), in which the correlation between two curves is based on the match of multiple stratigraphic trends and one core is used as "master curve". The correlation process is based on the Excel forecast function and linear regression between subsequent couples of selected tie-points. This process results in the estimate of the equivalent depth of the correlated curve (core2) in the depth scale of the "master" curve (core1). For the inner shelf core (17607-5), as stated above, only the upper 7.3 mbsf have been taken into account for the correlation; this interval was correlated with the topmost 5 m of Core 17603-3. The uppermost part of Core 17601-3 from the outer-shelf succession (between 0.35 and 2.18 mbsf) was correlated with the record of Core 17603-3 between 3.93 and 8.80 mbsf (Fig. 10a). The NRM and RPI trends of all three cores robustly matched (Fig. 10b,c). The ARM parameter shows a
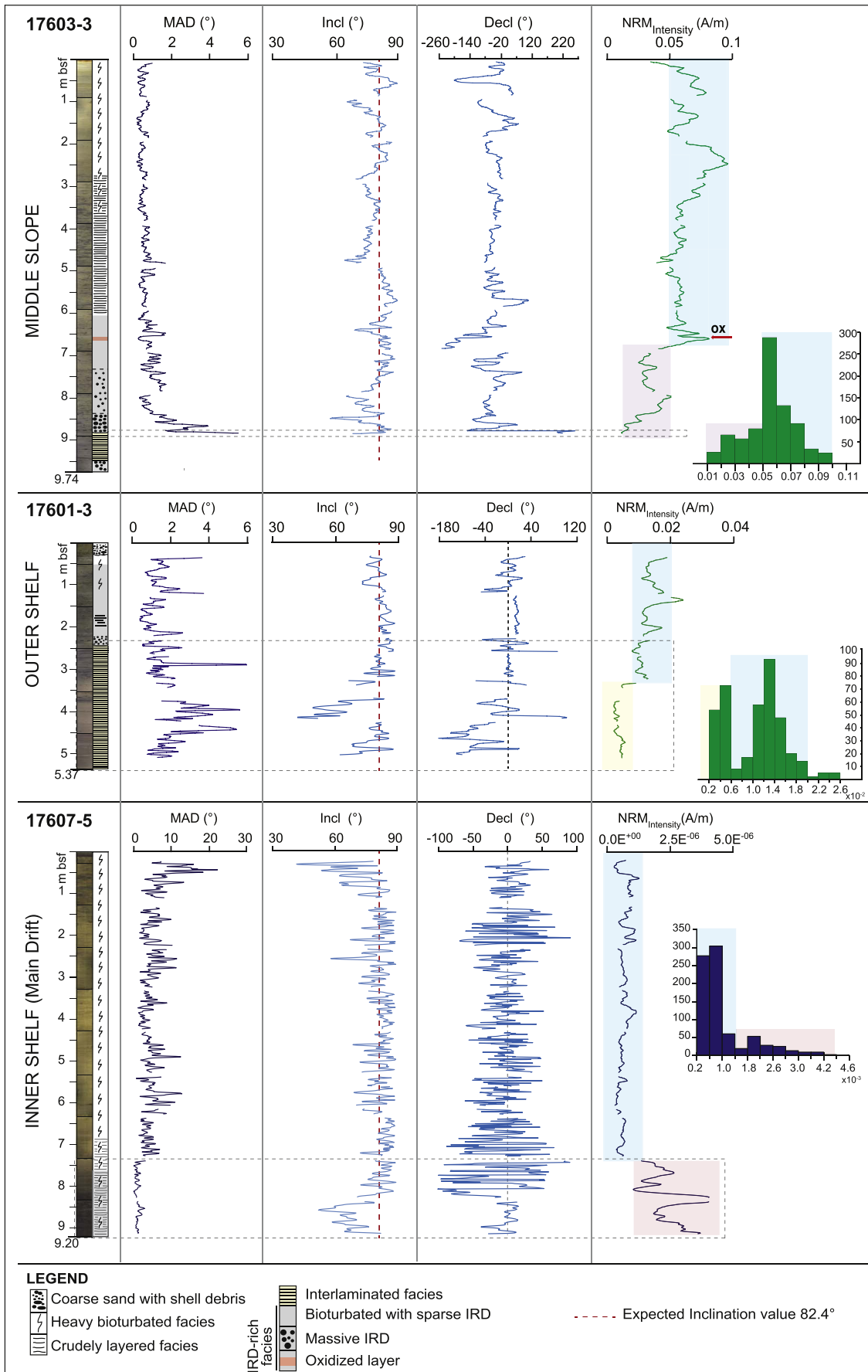
Fig. 8. Down-core variation of the maximum angular deviation (MAD), ChRM inclination, ChRM declination and natural remanent magnetization (NRM). A histogram representing the distribution of the measured values has been reported near the NRM graph. Areas in colour indicate corresponding stratigraphic intervals and ranges of NRM values. Dashed areas indicate intervals discarded for paleomagnetic interpretation.

strong match between Core 17601-3 and 17603-3, but a poor match between 17607-5 and 17603-3, because of the very low content in ferrimagnetic minerals in Core 17607-5 (Fig. 10d).

The lower 3 m of Core 17601-3 (represented in yellow in the log of Fig. 8) do not allow for a proper correlation with other cores. This interval corresponds to plumites deposited at an extremely high sedimentation rate as nearby SVAIS and EGLACOM cores showed. These plumites were previously interpreted to reflect a short time interval of high-accumulation in response to Meltwater Pulse 1a (MWP-1a; Fairbanks, 1989; Hanebuth et al., 2000), which lasted for about two centuries around 14.5 cal ka BP in this area (Lucchi et al., 2013, 2015; Sagnotti et al., 2016). This prominent event is recorded in the area with a large lateral variability in deposit thickness and onset ages depending on the depositional setting. As a matter of fact, the slope cores recorded only the initial phase of the melting event, when the sediment source (calving line) was located near the shelf edge. This initial phase of ice retreat may not be detectable in trough cores as this area was still covered by the ice stream. Meltwater sedimentation at the slope decreased with time while the glacial front retreated, and finally stopped at the time the calving line reached a critical distance for meltwater distribution (Hesse et al., 1997; Lucchi et al., 2002; Lucchi and Rebesco, 2007; Lucchi et al., 2013). From that time on, meltwater derived sediments settled on the continental shelf only. The meltwater record is therefore laterally discontinuous depending on the distance from the source area that retreated on land during time, so that the slope sequence is truncated at the top whereas the shelf (trough) sequence lacks

of the initial phase (onset) of this event. For said reasons we considered the record of the MWP-1a in the studied cores as a *marker bed* without further correlation within the event itself.

5.2. Age model

Starting from the constraints provided by the available AMS ^{14}C data set, we compared the paleomagnetic records for analyzed cores with the PSV and RPI variations expected at the cores location according to global and regional geomagnetic models (CALS7K.2 - Korte and Constable, 2005 - SHA.DIF.14k Pavón-Carrasco et al., 2014) and other records and stacks from high northern latitudes. Among the closest curves we take into account the UK PSV stack of Turner and Thompson, 1981, 1982; the FENNOSTACK by Snowball et al., 2007; the North Karelian Stack by the Haltia-Hovi et al., 2010; the EGLACOM-SVAIS stack by Sagnotti et al., 2011 and the Fennoscandian deglacial PSV master curve by Lougheed et al., 2014 (Fig. 11). These regional PSV stacks have been relocated to the CORIBAR core location by means of virtual geomagnetic pole (VGP) method (Noel and Batt, 1990). This method allows a direct comparison of the obtained paleomagnetic data with the paleomagnetic declination and inclination expected at the location of the analyzed cores according to the reference curves.

The RPI elements represent an additional valuable and original approach for time constrains and core correlation. The comparison of the RPI record indicates a close fit among the CORIBAR cores (blue scale) and the reference curve predicted by the SHA.DIF.14k and
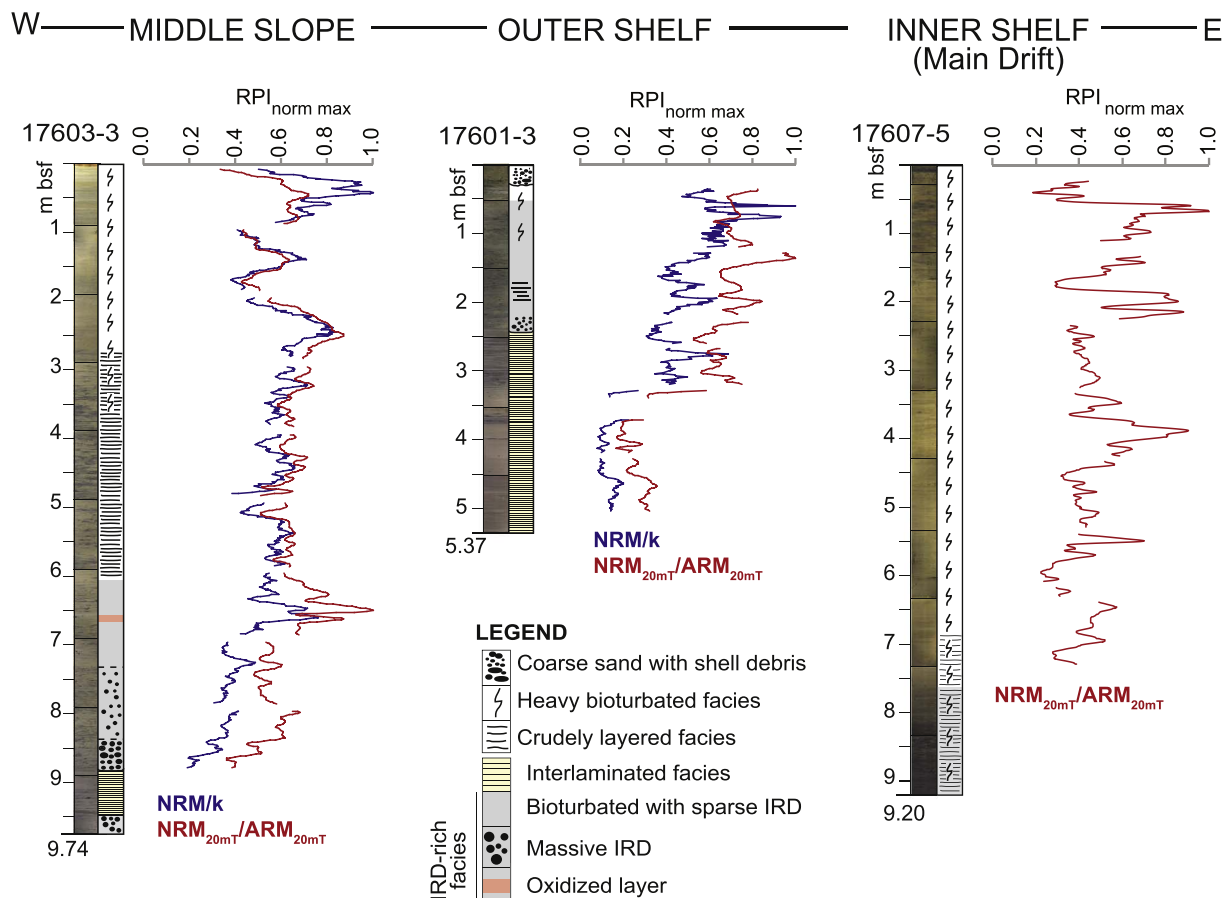
Fig. 9. Normalized relative paleointensity (RPI) curves, NRM/k, and NRM_{20mT}/ARM_{20mT}.
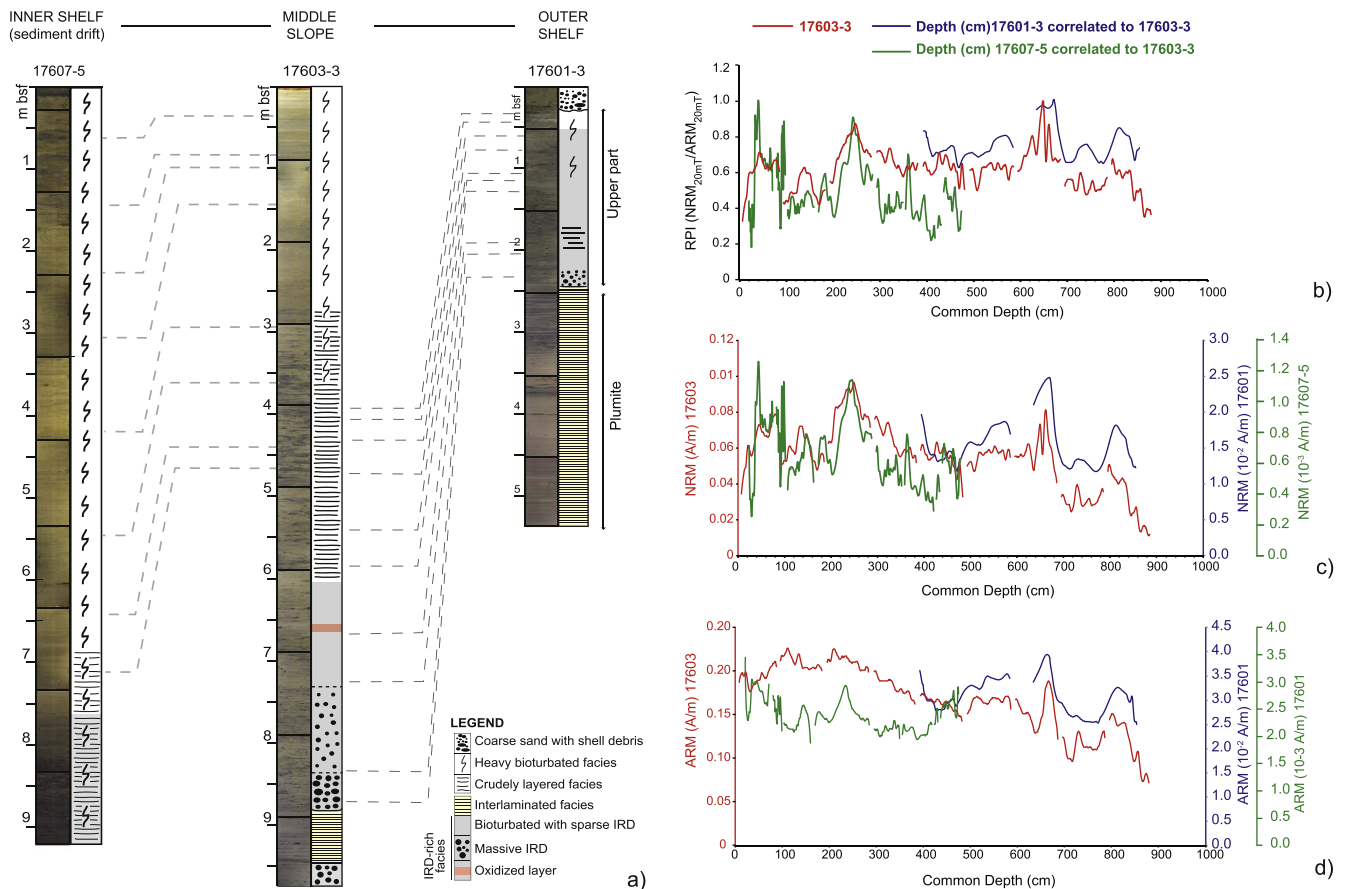
Fig. 10. a) Correlation of Core 17603-3, 17607-5 and 17601-3 stratigraphy, (b) relative paleointensity curves (RPI), c) natural remanent magnetization (NRM), d) anhysteretic remanent magnetization (ARM). Depths for 17607-05 (green) and 17601-3 (blue) have been converted to the stratigraphic depth of Core 17603-3 (red), which has the best paleomagnetic record and the highest available number of AMS ^{14}C calibrated ages (see Table 3 and Fig. 2). (For interpretation of the references to colour in this figure legend, the reader is referred to the web version of this article.)

CLAS7K.2 models (gray scale) (Fig. 11a). Moreover, a close match has been observed between slope core (17603–3) and EGLACOM-SVAIS stack, which was also derived from cores on the same continental slope. A broad RPI maximum is centered at around 2.10 cal ka BP and a broad minimum between ca. 5 and 8 cal ka BP (Fig. 11a). Cores 17607-1 and 17607-3 extend to ca. 14 cal ka BP, with another RPI maximum at ca. 12.4 cal ka BP. RPI reconstruction in Core 17607-5 is limited to the depth of 730 cm bsf (see Section 4.3) at ca. 11 cal ka BP. A radiocarbon dating on a scaphopod shell near the base of core indicates an age of ca. 10 cal ka BP.

The comparison of the ChRM inclination trends is shown in Fig. 11b. In detail, the inclination trend of Core 17601-3 remarkably matches with the predicted trend by SHA.DIF.14k model and the Fennoscandia stack (Fig. 11b). The inclination record from the slope core (17603-3) matches both with SHA.DIF.14k and CALS7K.2 models and with EGLACOM-SVAIS, North Karelian and Fennoscandia stacks. An apparent discrepancy is evident at the top of the inner-trough Core 17607-5 (Fig. 11b), with a pronounced inclination shallowing during the last 3 cal ka BP. This effect can, however, be explained with a poor paleomagnetic behavior in the uppermost 50 cm, as mentioned earlier. The rest of the core shows an inclination trend that matches with the SHA.DIF.14k and CALS7K.2 models.

The ChRM declination trend in the core from the inner shelf (17607-5-Fig. 11c) is not well-defined and shows high-frequency fluctuations, whereas declination trend for Cores 17603-3 and 17601-3 (Fig. 11c) is in reasonable agreement between the two cores and the models prediction and references stacks. Moreover, a large swing in ChRM declination is observed in Core 17603-3 between 2 and 3 cal ka BP

(Fig. 11c). This sharp declination change matches closely with the swing reported at the same age in the EGLACOM-SVAIS stack (Sagnotti et al., 2011), and corresponds to a sharp PSV change at 2.35–2.40 cal ka BP originally recognized by Turner and Thompson (1981, 1982) in lake sediments from Britain and named as the "f-e event". This feature indicates that the virtual geomagnetic pole VGP passed very close to the core site at 2.35–2.40 cal ka BP, when the ChRM is almost vertical.

The newly obtained paleomagnetic data confirm and support the efficiency of regional and global geomagnetic models to represent variability of the geomagnetic field at a high-resolution. Moreover, a general agreement has been observed among the CORIBAR core records and the stacks from the previous studies at high latitude. In particular a very close match has been observed with the EGLACOM-SVAIS stacks, whose records comes from cores collected in a very close area.

The CORIBAR data indicate that paleosecular variation of the geomagnetic field in the Holocene and late Pleistocene can be effectively used to trace changes and trends in declination, inclination and relative paleointensities, which are consistent both at a regional scale (i.e. Barents Sea) and at continental scale (i.e. Europe) and can therefore be used for correlating and dating of sedimentary sequences from different depositional settings. The paleomagnetic data from the continental shelf appear as particularly suitable to fidelity record the subtle variation of the geomagnetic field and provide an empirical estimate of secular variation intensity.
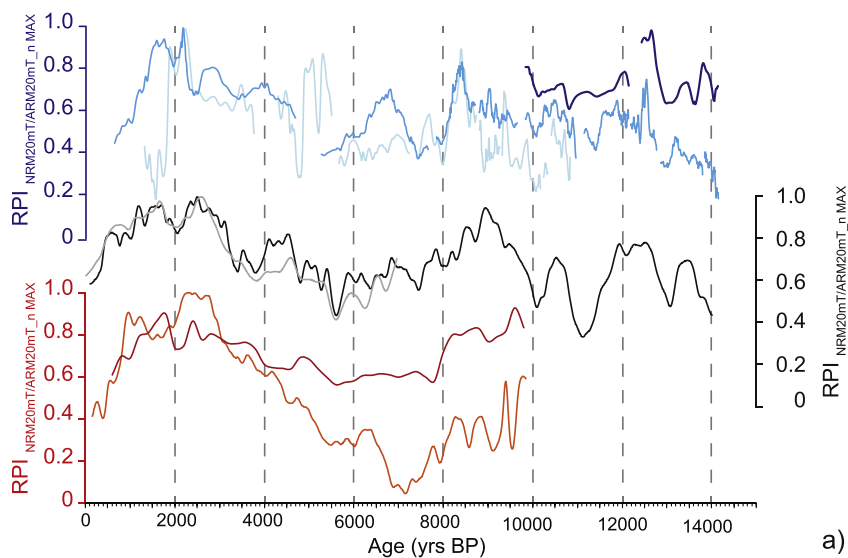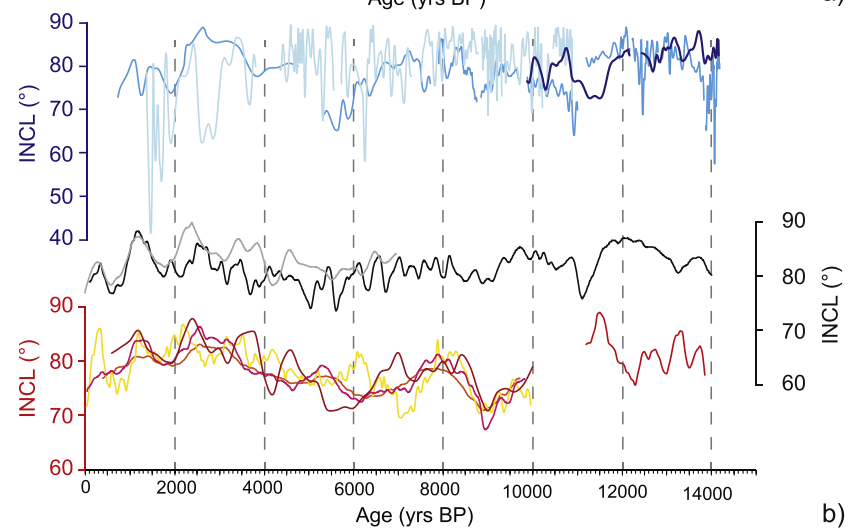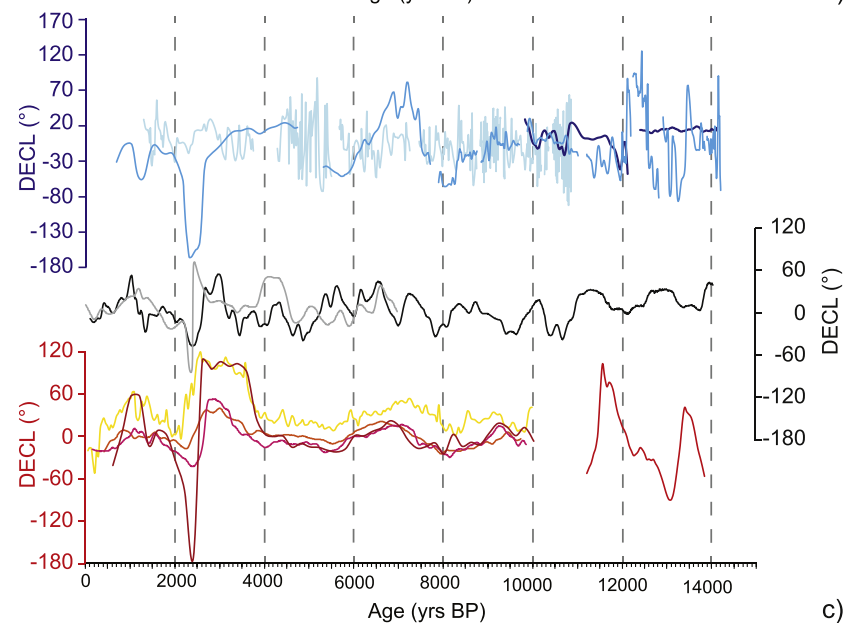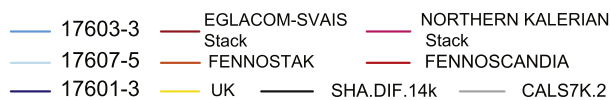
Fig. 11. RPI, ChRM inclinations and ChRM declinations of the CORIBAR cores (curves in blue scale) plotted as a function of age and compared with the FENNOSTAK, FENNOSCANDIA, UK, EGLACOM-SVAIS, Northern Kalerian stacks (curves in red scale) and predicted curves from the regional and global geomagnetic main field models SHA.DIF.14k and CALS7k.2 (curves in gray scale) (see the text for reference and discussions). (For interpretation of the references to colour in this figure legend, the reader is referred to the web version of this article.)
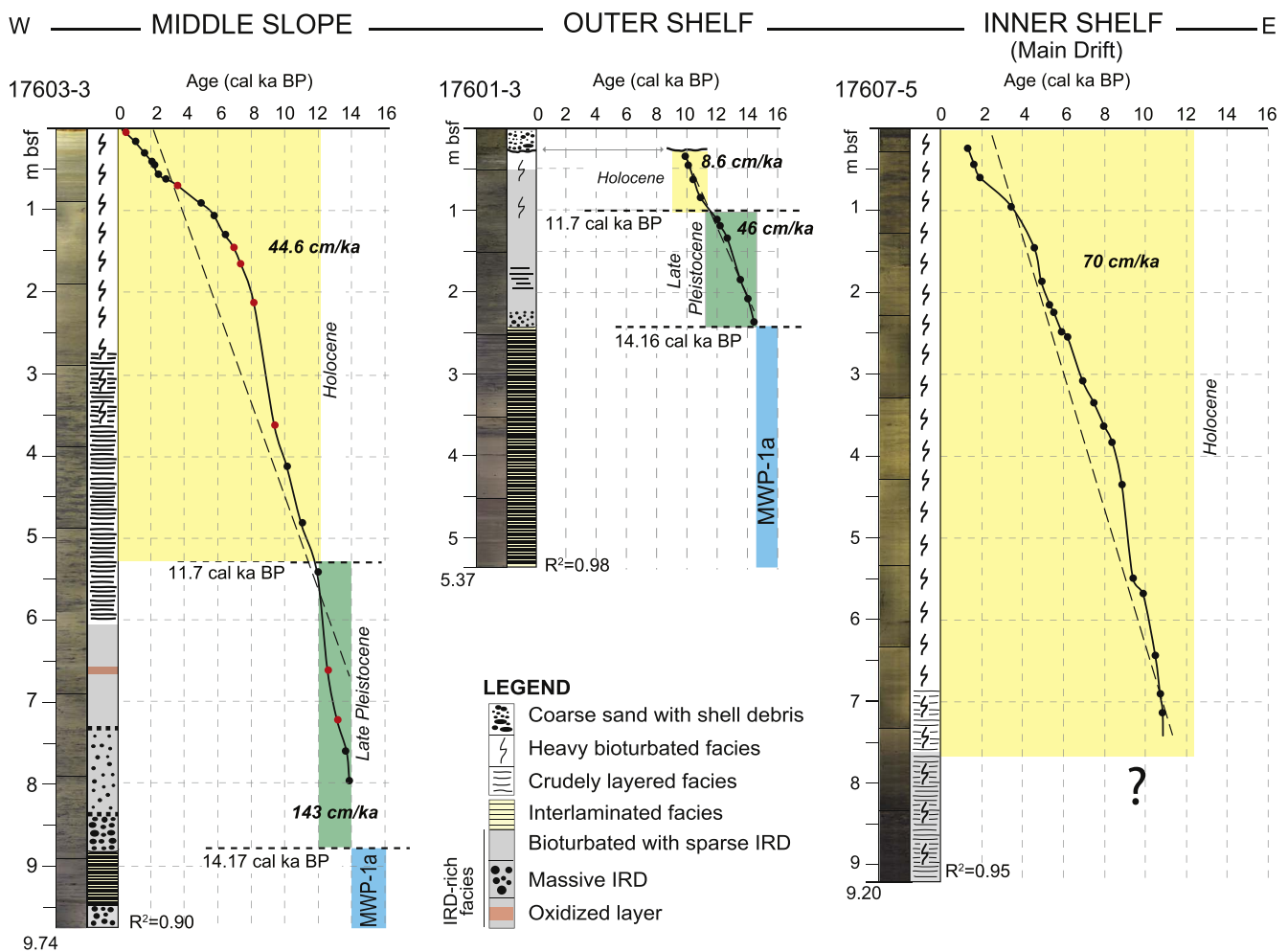
Fig. 12. Age model for Core 17603-3, 17601-3, and 17607-5 together with mean sedimentation rates for indicated intervals (yellow: Holocene; green: Late Pleistocene; light blue: Melt Water Pulse-1a event). Red dots indicate AMS ^{14}C ages from Core 17603-3; black dots indicate the tie-points identified by paleomagnetic and rock magnetic parameters correlations. The question mark indicates the uncertainties in the age model reconstruction for the interval of Core 17607-5 below 7.5 mbsf. The dashed lines indicate the linear regression of the age model with the respective R^2 values for each core. (For interpretation of the references to colour in this figure legend, the reader is referred to the web version of this article.)

5.3. Depositional evolution of the slope-shelf system

According to the reconstructed age model and core correlation, the outer-trough Core 17601-3 contains a thick (nearly 3 m) succession of laminated sediments (plumites) at its base that were associated with the MWP-1a event, which is also recorded at the base of the slope Core 17603-3. For the reasons explained above, we are considering the MWP-1a record as marker bed not allowing for any further detailed correlation. The post-MWP-1a sequence on both the middle TMF slope and outer shelf cores is composed by an interval of massive IRD, followed up-core by IRD-rich, bioturbated sediment that deposited with an average sedimentation rate of 143 cm/ka and 46 cm/ka, respectively, between 14.2 and 11.7 cal ka BP (Fig. 12). According to Lucchi et al. (2013, 2015), the massive IRD layer recovered on the slope record a major ice-sheet instability event occurred at the end (or during) the MWP-1a. Dating on the slope core confirms this hypothesis although it cannot give additional information on the timing of the ice-sheet collapse (during or at the end of the MWP-1a). The recovery of both plumites and the massive IRD layer on the outer Kveithola trough (Core 17601-3) clearly indicates that at least the outer trough area was ice-free or covered by a floating ice-shelf, with the grounding line located in a more landward location. Unfortunately, the inner trough Core 17607-5 recovered only the very late phase of deglaciation (since 12.4 cal ka BP) and cannot give more information about the grounding line location during MWP-1a.

On the middle slope, the IRD-rich facies is overlain by an expanded (> 5 m) Holocene sequence with respect to other areas of the Storfjorden-Kveithola TMF system (usually 1 to 4 m thick, e.g. Rasmussen et al., 2007; Jessen et al., 2010; Lucchi et al., 2013, among others), consisting of biogenic-rich, crudely layered and heavily bioturbated sediment. On the outer shelf on the contrary, the Holocene succession is about 1-m thick mainly consisting of terrigenous and bioturbated sediments that deposited at an average rate of only 8.6 cm/ka (compared to 44.6 cm/ka on the slope) (Fig. 12), and appears truncated at around 10 cal ka BP, by a bioclast-rich, pebbly sand lag deposit overlaying a sharp and irregular surface. We related the condensed Holocene sedimentary sequence in the outer Kveithola Trough with the presence of strong bottom currents likely associated with the main core of the West Spitsbergen Current presently located between 200 and 400 m water depth (Aagaard et al., 1985; Osinski et al., 2003).

In contrast, the slope Core 17603-3 was recovered from a depocenter, where sediment accumulated under the synergic effect of slow along slope contour currents generating crude sediment layering, and across-slope dense bottom currents supplying sediments from the shelf area (the Turbid and Saline flows named *TS plumes* by Fohrmann et al., 1998). In this respect, the slope area of site 17603-3 can be considered as an *embryonic* sediment drift sharing onset and development characteristics with the Bellsund and Isfjorden sediment drifts studied along the Svalbard western margin (Rebesco et al., 2014; Lantzsch et al., 2017).

Core 17607-5 located on the Kveithola Main Sediment Drift (inner trough) contains a very expanded Holocene sequence mainly composed of medium-sized, bioturbated, bioclast-rich sandy silts, with an overall textural fining up-core trend. This interval was deposited at an average sedimentation rate of 70 cm/ka. The lower part of the core (between 9.2 and 7.6 mbsf) is composed by finely bioturbated terrigenous silt with coarse sediment bedding. According to the sediment facies analyses, both terrigenous silt and biogenic sands deposited under persistent bottom currents linked to the Kveithola Main Sediment Drift formation. According to the age model, the gradual change between the terrigenous silt and the biogenic sands occurred around 10.6 cal ka BP. We infer that a drastic change in the sources of terrigenous input occurred during this time, likely associated to the local glacial drainage system with a substantial shrinking of the remaining marginal ice-sheets including the possible ice caps on the nearby Spitsbergenbanken and Bear Island. This interpretation is coherent with the timing of the sharp compositional change observed in the both CORIBAR Core 17623-2, located on the Spitsbergenbanken where the rapid change dates ca. 9 cal ka BP (Zecchin et al., 2016), and Core SV-06, located on the neighboring Storfjorden Trough in which a sharp compositional change dates ca. 9.5 cal ka BP (Sagnotti et al., 2011). The impossibility of reconstructing a reliable high resolution age model based on paleomagnetic and rock magnetic parameters in the sediments located at the base of Core 17607-5, ruled out the possibility of adding any further information about the onset and sedimentological evolution of the Kveithola Main Sediment Drift. It is, however, unclear how contour currents in the Kveithola Drift can be responsible for organic matter rich sedimentation with low benthic fauna diversification and development of opportunistic living species indicating reducing, or even anoxic, environmental conditions (Hanebuth et al., 2013; Sabbatini et al., 2017). The sedimentation under contour currents is usually characterized by highly populated benthic fauna in well-oxygenated environmental conditions, since contour currents transport not only sediments but also oxygen and nutrients (Rebesco and Camerlenghi, 2008, and references therein). While more investigation are needed to solve such an apparently contradictory depositional environment, we speculate that the local oceanographic configuration may have played an important role through water stratification caused by the presence of winter brine formation, spring/summer cold fresh water release from sea ice melting, and summer shelf inflow of the warm and saline Western Spitsbergen Current. Strong water mass stratification would have prevented vertical gas exchange and bottom ventilation necessary for benthic fauna consumption of the organic matter, driving to the onset of oxygen-reduced conditions and development of opportunistic benthic species.

6. Conclusion

We report new paleomagnetic and rock magnetic data from cores collected along a continental shelf-to-slope transect in the Kveithola Trough and TMF, NW Barents Sea. The sediment cores are characterized by high-quality paleomagnetic and rock magnetic properties and a well-defined characteristic remanent magnetization (ChRM) throughout most of the retrieved sequences. These allow high-resolution correlation between the shelf-slope sedimentary successions and the estimate of relative paleointensity (RPI) variation of geomagnetic field. Moreover our paleomagnetic results from Holocene and late Pleistocene deposits confirm and support the SHA.DIF.14k model to represent geomagnetic field variability at a high-resolution, and indicate that RPI is a valuable approach for time constrains and core correlation. Moreover a close match among CORIBAR records and the available stacks at high latitude have been observed especially with the EGLACOM-SVAIS stack.

The time framework provided by the age model corroborated by the ^{14}C ages, constrains the depositional evolution of the Kveithola slope to shelf glacigenic system during the past 15 thousand years. The

presence, on the outer trough, of the plumites and the massive IRD layer associated to the MWP-1a and collapse of the ice-stream respectively, indicates that at least the outer trough area was ice-free or covered by a floating ice-shelf, with the grounding line located in a more landward location within the trough. The inner trough core located on the Kveithola Main Sediment Drift, recovered a very expanded Holocene sequence. A rapid compositional change within the core from terrigenous to biogenic sediments suggests a drastic change in the sediment source likely to be associated to the final shrinking of relict, marginal ice-sheets, possibly including the ice caps on the nearby Spitsbergenbanken and Bear Island. In conclusion, this study highlights the large potential of rock magnetic and paleomagnetic analyses for sedimentary reconstructions during the glacial-deglacial history at polar continental margins. By combining these methods with sedimentological analyses, a reconstruction of glacigenic processes and paleoceanographic variability due to climatic changes during the past 15 thousand years has been attained.

References

Aagaard, K., Swift, J.H., Carmack, E.C., 1985. Thermohaline circulation in the arctic Mediterranean seas. J. Geophys. Res. 90, 4833–4846. http://dx.doi.org/10.1029/JC090iC03p04833.

Alley, R.B., Blankenship, D.D., Rooney, S.T., Bentley, C.R., 1989. Sedimentation beneath ice shelves–the view from ice stream B. Mar. Geol. 85, 101–120. http://dx.doi.org/10.1016/0025-3227(89)90150-3.

Banerjee, S.K., King, J., Marvin, J., 1981. A rapid method for magnetic granulometry with applications to environmental studies. Geophys. Res. Lett. 8, 333–336. http://dx.doi.org/10.1029/GL008i004p00333.

Bartington Instruments Ltd., 2002. Operation Manual for MS2 Magnetic Susceptibility System. OM408 Issue 27, Oxford, UK, 67.

Bjarnadóttir, L.R., Rüther, D.C., Winsborrow, M.C.M., Andreassen, K., 2013. Grounding-line dynamics during the last deglaciation of Kveithola, W Barents Sea, as revealed by seabed geomorphology and shallow seismic stratigraphy. Boreas 42, 84–107. http://dx.doi.org/10.1111/j.1502-3885.2012.00273.x.

Brachfeld, S.A., 2006. High-field magnetic susceptibility (χHF) as a proxy of biogenic sedimentation along the Antarctic Peninsula. Phys. Earth Planet. Inter. 156, 274–282. http://dx.doi.org/10.1016/j.pepi.2005.06.019.

Brachfeld, S., Banerjee, S.K., Guyodo, Y., Acton, G.D., 2002. A 13,200 year history of century to millennial scale paleoenvironmental change magnetically recorded in the Palmer Deep, western Antarctic Peninsula. Earth Planet. Sci. Lett. 194, 311–326. http://dx.doi.org/10.1016/S0012-821X(01)00567-2.

Brachfeld, S., Kissel, C., Laj, C., Mazaud, A., 2004. Behavior of u-channels during acquisition and demagnetization of remanence: implications for paleomagnetic and rock magnetic measurements. Phys. Earth Planet. Inter. 145, 1–8. http://dx.doi.org/10.1016/j.pepi.2003.12.011.

Brachfeld, S., Barletta, F., St-Onge, G., Darby, D., Ortiz, J.D., 2009. Impact of diagenesis on the environmental magnetic record from a Holocene sedimentary sequence from the Chukchi–Alaskan margin, Arctic Ocean. Glob. Planet. Chang. 68, 100–114. http://dx.doi.org/10.1016/j.gloplacha.2009.03.023.

Brachfeld, S., Pinzon, J., Darley, J., Sagnotti, L., Kuhn, G., Florindo, F., Wilson, G.,

Ohneiser, C., Monien, D., Joseph, L., 2013. Magnetic tracers of ice sheet extent and sediment provenance in the ANDRILL AND-1B drill Core, Ross Sea, Antarctica. Glob. Planet. Chang. 110, 420–433.

Carbonara, K., Mezgec, K., Varagona, G., Musco, M.E., Lucchi, R.G., Villa, G., Morigi, C., Melis, R., Caffau, M., 2016. Palaeoclimatic changes in Kveithola, Svalbard, during the Late Pleistocene deglaciation and Holocene: evidences from microfossil and sedimentary records. Palaeogeogr. Palaeoecol. 463, 136–149. http://dx.doi.org/10.1016/j.palaeo.2016.10.003.

Dearing, J.A., 1999. Holocene environmental change from magnetic proxies in lake sediments. In: Maher, Barbara A., Thompson, Roy (Eds.), Quaternary Climates, Environments and Magnetism. Cambridge University Press.

Donadini, F., Korte, M., Constable, C.G., 2009. Geomagnetic field for 0–3 ka: 1. New data sets for global modeling. Geochem. Geophys. Geosyst. 10. http://dx.doi.org/10.1029/2008GC002295.

Dowdeswell, J.A., Ottesen, D., Evans, J., Cofaigh, C.Ó., Anderson, J.B., 2008. Submarine glacial landforms and rates of ice-stream collapse. Geology 36, 819–822. http://dx.doi.org/10.1130/G24808A.1.

Elverhøi, A., Andersen, E.S., Dokken, T., Hebbeln, D., Spielhagen, R., Svendsen, J.I., Sørflaten, M., Rørnes, A., Hald, M., Forsberg, C.F., 1995. The growth and decay of the Late Weichselian ice sheet in western Svalbard and adjacent areas based on provenance studies of marine sediments. Quat. Res. 44, 303–316. http://dx.doi.org/10.1006/qres.1995.1076.

Fairbanks, R.G., 1989. A 17.000-year glacio-eustatic sea level record: influence of glacial melting rates on the younger Dryas event and deep-ocean circulation. Nature 342, 637–642.

Fohrmann, H., Backhaus, J.O., Blaume, F., Rumohr, J., 1998. Sediments in bottom arrested gravity plumes: numerical case studies. J. Phys. Oceanogr. 28, 2250–2274. http://dx.doi.org/10.1175/1520-0485(1998)028<2250:SIBAGP>2.0.CO;2.

Fu, Y., von Dobeneck, T., Franke, C., Heslop, D., Kasten, S., 2008. Rockmagnetic identification and geochemical process models of greigite formation in Quaternary marine sediments from the Gulf of Mexico (IODP Hole U1319A). Earth Planet. Sci. Lett. 275 233–24. https://doi.org/10.1016/j.epsl.2008.07.034.

Gee, J., Staudigel, H., Tauxe, L., Pick, T., 1993. Magnetization of the La Palma seamount series: implications for seamount paleopoles. J. Geophys. Res. 98, 11743–11767. http://dx.doi.org/10.1029/93JB00932.

Gordon, D.C., 1970. A microscopic study of organic particles in the North Atlantic Ocean. Deep-Sea Res. 17, 175–185. http://dx.doi.org/10.1016/0011-7471(70)90096-3.

Hagstrum, J.T., Champion, D.E., 2002. A Holocene paleosecular variation record from 14C-dated volcanic rocks in western North America. J. Geophys. Res. 107, 2025. http://dx.doi.org/10.1029/2001JB000524.

Haltia-Hovi, E., Nowaczyk, N., Saarinen, T., 2010. Holocene palaeomagnetic secular variation recorded in multiple lake sediment cores from eastern Finland. Geophys. J. Int. 180, 609–622. http://dx.doi.org/10.1111/j.1365-246X.2009.04456.x.

Hanebuth, T.J.J., Stattegger, K., Grootes, P.M., 2000. Rapid flooding of the Sunda Shelf: a late-glacial sea-level record. Science 288, 1033–1035. http://dx.doi.org/10.1126/science.288.5468.1033.

Hanebuth, T.J.J., Lantzsch, H., Bergenthal, M., Caburlotto, A., Dippold, S., Düßmann, R., Freudenthal, T., Hörner, T., Kaszemeik, K., Klar, S., Llopart, J., Lucchi, R.G., Nicolaisen, L.S., Noorlander, K., Osti, G., Özmaral, A., Rebesco, M., Rosiak, U., Sabbatini, A., Schmidt, W., Stachowski, A., Urgeles, R., 2013. CORIBAR – Ice dynamics and meltwater deposits: coring in the Kveithola Trough, NW Barents Sea. Cruise MSM30, 16.07–15.08.2013, Tromsø (Norway) – Tromsø (Norway). Berichte 299 (74), 2195–7894 MARUM – Zentrum fur Marine Umweltwissenschaften, Fachbereich Geowissenschaften, Universität Bremen.

Hanebuth, T.J.J., Rebesco, M., Urgeles, R., Lucchi, R.G., Freudenthal, T., 2014. Drilling glacial deposits in offshore polar regions. EOS Trans. Am. Geophys. Union 95, 277–284. http://dx.doi.org/10.1002/2014EO310001.

Hesse, R., Khodabakhsh, S., Klauck, I., Ryan, W.B.F., 1997. Asymmetrical turbid surface-plume deposition near ice-outlets of the Pleistocene Laurentide ice sheet in the Labrador Sea. Geo-Mar. Lett. 17, 179–187.

Hounslow, M.W., Morton, A.C., 2004. Evaluation of sediment provenance using magnetic mineral inclusions in clastic silicates: comparison with heavy mineral analysis. Sediment. Geol. 171, 13–36. http://dx.doi.org/10.1016/j.sedgeo.2004.05.008.

Jessen, S.P., Rasmussen, T.L., Nielsen, T., Solheim, A., 2010. A new Late Weichselian and Holocene marine chronology for the western Svalbard slope 30,000–0 cal years BP. Quat. Sci. Rev. 29, 1301–1312. http://dx.doi.org/10.1016/j.quascirev.2010.02.020.

King, J.W., Banerjee, S.K., Marvin, J., Özdemir, Ö., 1982. A comparison of different magnetic methods for determining the relative grain size of magnetite in natural materials: some results from lake sediments. Earth Planet. Sci. Lett. 59, 404–419. http://dx.doi.org/10.1016/0012-821X(82)90142-X.

King, J.W., Banerjee, S.K., Marvin, J., 1983. A new rock-magnetic approach to selecting sediments for geomagnetic paleointensity for the last 4000 years. J. Geophys. Res. 88, 5911–5921. http://dx.doi.org/10.1029/JB088iB07p05911.

Kirschvink, J.L., 1980. The least-squares line and plane and the analysis of paleomagnetic data. Geophys. J. Int. 62, 699–718. http://dx.doi.org/10.1111/j.1365-246X.1980.tb02601.x.

Kissel, C., Laj, C., Lehman, B., Labyrie, L., Bout-Roumazeilles, V., 1997. Changes in the strength of the Iceland–Scotland overflow water in the last 200,000 years: evidence from magnetic anisotropy analysis of core SU90-33. Earth Planet. Sci. Lett. 152, 25–36. http://dx.doi.org/10.1016/S0012-821X(97)00146-5.

Kissel, C., Laj, C., Labeyrie, L., Dokken, T., Voelker, A., Blamart, D., 1999. Rapid climatic variations during marine isotopic stage 3: magnetic analysis of sediments from Nordic seas and North Atlantic. Earth Planet. Sci. Lett. 171, 489–502. http://dx.doi.org/10.1016/S0012-821X(99)00162-4.

Kissel, C., Laj, C., Clemens, S., Solheid, P., 2003. Magnetic signature of environmental changes in the last 1.2 Myr at ODP site 1146, South China Sea. Mar. Geol. 201, 119–132. http://dx.doi.org/10.1016/S0025-3227(03)00212-3.

Korte, M., Constable, C.G., 2005. The geomagnetic dipole moment over the last 7000 years—new results from a global model. Earth Planet. Sci. Lett. 236, 348–358. http://dx.doi.org/10.1016/j.epsl.2004.12.031.

Korte, M., Genevey, A., Constable, C.G., Frank, U., Schnepp, E., 2005. Continuous geomagnetic field models for the past 7 millennia: 1. A new global data compilation. Geochem. Geophys. Geosyst. 6. http://dx.doi.org/10.1029/2004GC000800.

Korte, M., Donadini, F., Constable, C., 2009. Geomagnetic field for 0–3 ka: 2. A new series of time-varying global models. Geochem. Geophys. Geosyst. 10, Q06008. http://dx.doi.org/10.1029/2008GC002297.

Laberg, J.S., Stoker, M.S., Dahlgren, K.I.T., de Haas, H., Haflidason, H., Hjelstuen, B.O., Nielsen, T., Shannon, P.M., Vorren, T.O., vanWeering, T., Ceramicola, S., 2005. Cenozoic along slope processes and sedimentation on the NW European Atlantic margin. Mar. Pet. Geol. 22, 1069–1088. http://dx.doi.org/10.1016/j.marpetgeo.2005.01.008.

Lantzsch, H., Hanebuth, T.J.J., Horry, J., Grave, M., Rebesco, M., Schwenk, T., 2017. Deglacial to Holocene history of ice-sheet retreat and bottom current strength on the western Barents Sea shelf. Quat. Sci. Rev. 173, 40–57. http://dx.doi.org/10.1016/j.quascirev.2017.08.016.

Larrasoaña, J.C., Roberts, A.P., Stoner, J.S., Richter, C., Wehausen, R., 2003. A new proxy for bottom-water ventilation in the eastern Mediterranean based on diagenetically controlled magnetic properties of sapropel-bearing sediments. Palaeogeogr. Palaeoecol. 190, 221–242. http://dx.doi.org/10.1016/S0031-0182(02)00607-7.

Larrasoaña, J.C., Roberts, A.P., Musgrave, R.J., Gràcia, E., Piñero, E., Vega, M., Martínez-Ruiz, F., 2007. Diagenetic formation of greigite and pyrrhotite in gas hydrate marine sedimentary systems. Earth Planet. Sci. Lett. 261, 350–366. http://dx.doi.org/10.1016/j.epsl.2007.06.032.

Leslie, B.W., Hammond, D.E., Berelson, W.M., Lund, S.P., 1990. Diagenesis in anoxic sediments from the California continental borderland and its influence on iron, sulfur and magnetite behavior. J. Geophys. Res. 95, 4453–4470. http://dx.doi.org/10.1029/JB095iB04p04453.

Liu, Q., Roberts, A.P., Larrasoaña, J.C., Banerjee, S.K., Guyodo, Y., Tauxe, L., Oldfield, F., 2012. Environmental magnetism: principles and applications. Rev. Geophys. 50, RG4002. http://dx.doi.org/10.1029/2012RG000393.

Llopart, J., Urgeles, R., Camerlenghi, A., Lucchi, R.G., De Mol, B., Rebesco, M., Pedrosa, M.T., 2016. Slope instability of glaciated continental margins: constraints from permeability-compressibility tests and hydrogeological modeling off Storfjorden, NW Barents Sea. In: Krastel, S. (Ed.), Submarine Mass Movements and Their Consequences, Advances in Natural and Technological Hazards Research. 37. Springer Science Book Series, pp. 95–104.

Lougheed, B.C., Nilsson, A., Björck, S., Snowball, I., Muscheler, R., 2014. A deglacial palaeomagnetic master curve for Fennoscandia - providing a dating template and supporting millennial-scale geomagnetic field patterns for the past 14 ka. Quat. Sci. Rev. 106, 155–166. http://dx.doi.org/10.1016/j.quascirev.2014.03.008.

Lucchi, R.G., Rebesco, M., 2007. Glacial contourites on the Antarctic peninsula margins: insight for palaeoenvironmental and palaeoclimatic conditions. In: Viana, A.R., Rebesco, M. (Eds.), Economic and Palaeosignificance of Contourite Deposits. Geological Society of London Special Publication 276. pp. 111–127. http://dx.doi.org/10.1144/GSL.SP.2007.276.01.06.

Lucchi, R.G., Rebesco, M., Camerlenghi, A., Busetti, M., Tomadin, L., Villa, G., Persico, D., Morigi, C., Bonci, M.C., Giorgetti, G., 2002. Glacimarine sedimentary processes of a high-latitude, deep-sea sediment drift (Antarctic Peninsula Pacific margin). Mar. Geol. 189, 343–370. http://dx.doi.org/10.1016/S0025-3227(02)00470-X.

Lucchi, R.G., Camerlenghi, A., Rebesco, M., Colmenero-Hidalgo, E., Sierro, F.J., Sagnotti, L., Urgeles, R., Melis, R., Morigi, C., Bárcena, M.-A., Giorgetti, G., Villa, G., Persico, D., Flores, J.-A., Rigual-Hernández, A.S., Pedrosa, M.T., Macri, P., Caburlotto, A., 2013. Postglacial sedimentary processes on the Storfjorden and Kveithola trough mouth fans: significance of extreme glacimarine sedimentation. Glob. Planet. Chang. 111, 309–326. http://dx.doi.org/10.1016/j.gloplacha.2013.10.008.

Lucchi, R.G., Sagnotti, L., Camerlenghi, A., Macrì, P., Pedrosa, M.T., Giorgetti, G., 2015. Marine sedimentary record of meltwater pulse 1a along the NW Barents Sea continental margin. Ark. Dent. 1, 7.

Maher, B.A., 1988. Magnetic properties of some synthetic sub-micron magnetites. Geophys. J. R. Astron. Soc. 94, 83–96. http://dx.doi.org/10.1111/j.1365-246X.1988.tb03429.x.

Mangerud, J., Gulliksen, S., 1975. Apparent radiocarbon ages of recent marine shells from Norway, Spitsbergen, and Arctic Canada. Quat. Res. 5, 263–273. http://dx.doi.org/10.1016/0033-5894(75)90028-9.

Mangerud, J., Dokken, T., Hebbeln, D., Heggen, B., Ingólfsson, Ó., Landvik, J.Y., Mejdahl, V., Svendsen, J.I., Vorren, T.O., 1998. Fluctuations of the Svalbard–Barents sea ice sheet during the last 150,000 years. Quat. Sci. Rev. 17, 11–42. http://dx.doi.org/10.1016/S0277-3791(97)00069-3.

Muhs, D.R., Reynolds, R., Been, J., Skipp, G., 2003. Eolian sand transport pathways in the southwestern United States: importance of the Colorado River and local sources. Quat. Sci. Rev. 104, 3–18. http://dx.doi.org/10.1016/S1040-6182(02)00131-3.

Nieuwenhuize, J., Maas, Y.E.M., Middelburg, J.J., 1994. Rapid analysis of organic carbon and nitrogen in particulate materials. Mar. Chem. 45, 217–224. http://dx.doi.org/10.1016/0304-4203(94)90005-1.

Noel, M., Batt, C.M., 1990. A method for correcting geo-graphically separated remanence directions for the purpose of archeomagnetic dating. Geophys. J. Int. 102, 753–756. http://dx.doi.org/10.1111/j.1365-246X.1990.tb04594.x.

Nowaczyk, N., Haewart, S., Melles, M., 2000. A rock magnetic record from Lama Lake, Taymyr Peninsula, northern Central Siberia. J. Paleolimnol. 23, 223–241.

Osinski, R., Wieczorek, P., Beszczynska-Moeller, A., Goszczko, I., 2003. ADCP-referenced geostrophic velocity and transport in the West Spitsbergen Current. Oceanologia 45, 425–435.

Pavón-Carrasco, F.J., Osete, M.L., Torta, J.M., De Santis, A., 2014. A geomagnetic field model for the Holocene based on archeomagnetic and lava flow data. Earth Planet. Sci. 338, 98–109. http://dx.doi.org/10.1016/j.epsl.2013.11.046.

Pedrosa, M., Camerlenghi, A., De Mol, B., Urgeles, R., Rebesco, M., Lucchi, R.G., SVAIS, EGLACOM Cruises shipboard parties, 2011. Seabed morphology and shallow sedimentary structure of the Storfjorden and Kveithola trough-mouth fans (north west Barents Sea). Mar. Geol. 286, 65–81. http://dx.doi.org/10.1016/j.margeo.2011.05.009.

Rasmussen, T.L., Thomsen, E., Ślubowska, M.A., Jessen, S., Solheim, A., Koç, N., 2007. Paleoceanographic evolution of the SW Svalbard margin (76°N) since 20,000 14C yr BP. Quat. Res. 67, 100–114. http://dx.doi.org/10.1016/j.yqres.2006.07.002.

Rebesco, M., Camerlenghi, A., 2008. Contourites. Developments in Sedimentology 60. Elsevier Science, pp. 663.

Rebesco, M., Liu, Y., Camerlenghi, A., Winsborrow, M., Laberg, J.S., Caburlotto, A., Diviacco, P., Accettella, D., Sauli, C., Wardell, N., Tomini, I., 2011. Deglaciation of the western margin of the Barents Sea ice sheet — a swath bathymetric and sub-bottom seismic study from the Kveithola trough. Mar. Geol. 279, 141–147. http://dx.doi.org/10.1016/j.margeo.2010.10.018.

Rebesco, M., Laberg, J.S., Pedrosa, M.T., Camerlenghi, A., Lucchi, R.G., Zgur, F., Wardell, N., 2014. Onset and growth of trough-mouth fans on the north-western Barents Sea margin–implications for the evolution of the Barents Sea/Svalbard ice sheet. Quat. Sci. Rev. 92, 227–234. http://dx.doi.org/10.1016/j.quascirev.2013.08.015.

Rebesco, M., Özmaral, A., Urgeles, R., Accettella, A., Lucchi, R.G., Rüther, D., Winsborrow, M., Llopart, J., Caburlotto, A., Lanztzsch, H., Hanebuth, Till J.J., 2016. Evolution of a high-latitude sediment drift inside a glacially-carved trough based on high-resolution seismic stratigraphy (Kveithola, NW Barents Sea). Quat. Sci. Rev. 147, 178–193. http://dx.doi.org/10.1016/j.quascirev.2016.02.007.

Reimer, P., 2013. IntCal13 and Marine13 radiocarbon age calibration curves 0–50,000 years cal BP. Radiocarbon 55, 1869–1887. http://dx.doi.org/10.2458/azu_js.rc.55.16947.

Roberts, A.P., 2006. High-resolution magnetic analysis of sediment cores: strengths, limitations and strategies for max-imizing the value of long-core magnetic data. Phys. Earth Planet. Inter. 156, 162–178. http://dx.doi.org/10.1016/j.pepi.2005.03.021.

Roberts, A.P., 2015. Magnetic mineral diagenesis. Earth-Sci. Rev. 151, 1–47. http://dx.doi.org/10.1016/j.earscirev.2015.09.010.

Robinson, S.G., 1986. The late Pleistocene palaeoclimatic record of North Atlantic deepsea sediments revealed by mineral-magnetic measurements. Phys. Earth Planet. Inter. 42, 22–47. http://dx.doi.org/10.1016/S0031-9201(86)80006-1.

Rothwell, R.G., Hoogakker, B., Thomson, J., Croudace, I.W., Frenz, M., 2006. Turbidite emplacement on the southern Balearic abyssal plain (western Mediterranean Sea) during marine isotope stages 1–3: an application of ITRAX XRF scanning of sediment cores to lithostratigraphic analysis. In: Rothwell, R.G. (Ed.), New Techniques in Sediment Core Analysis. Geol. Soc. Spec. Publ. 267. pp. 79–98. http://dx.doi.org/10.1144/GSL.SP.2006.267.01.06.

Rousse, S., Kissel, C., Laj, C., Eiríksson, J., Knudsen, K.-L., 2006. Holocene centennial to millennial-scale climatic variability: evidence from high-resolution magnetic analyses of the last 10 cal kyr off North Iceland (core MD99-2275). Earth Planet. Sci. Lett. 242, 390–405. http://dx.doi.org/10.1016/j.epsl.2005.07.030.

Rüther, D.C., Bjarnadóttir, L.R., Junttila, J., Husum, K., Rasmussen, T.L., Lucchi, R.G., Andreassen, K., 2012. Pattern and timing of the northwestern Barents Sea ice sheet deglaciation and indications of episodic Holocene deposition. Boreas 41, 494–512. http://dx.doi.org/10.1111/j.1502-3885.2011.00244.x.

Sabbatini, A., Morigi, C., Lucchi, R.G., De Vittor, C., the scientific party of the CORIBAR project, 2017. Living (rose-bengal-stained) benthic foraminifera along the Kveithola trough (NW Barents Sea), environmental implications. In: Geophysical Research Abstracts. Vol. 19. EGU General Assembly, pp. 2017 EGU2017-12487-1.

Sagnotti, L., 2011. Magnetic anisotropy. In: Grupta, H.K. (Ed.), Encyclopedia of Solid Earth Geophysics. Springer.

Sagnotti, L., 2013. Demagnetization analysis in Excel (DAIE)—an open source workbook in Excel for viewing and analyzing demagnetization data from paleomagnetic discrete samples and u-channels. Ann. Geophys. Italy 56, D0114. http://dx.doi.org/10.4401/ag-6282.

Sagnotti, L., Macrí, P., Camerlenghi, A., Rebesco, M., 2001. Environmental magnetism of Antarctic Late Pleistocene sediments and interhemispheric correlation of climatic events. Earth Planet. Sci. Lett. 192, 65–80. http://dx.doi.org/10.1016/S0012-821X(01)00438-1.

Sagnotti, L., Rochette, P., Jackson, M., Vadeboin, F., Dinarès-Turell, J., Winkler, A., 2003. "Mag-Net" science team, inter-laboratory calibration of low field and anhystereticsusceptibility measurements. Phys. Earth Planet. Inter. 138, 25–38. http://dx.doi.org/10.1016/S0031-9201(03)00063-3.

Sagnotti, L., Macrì, P., Lucchi, R., Rebesco, M., Camerlenghi, A., 2011. A Holocene paleosecular variation record from the northwestern Barents Sea continental margin. Geochem. Geophys. Geosyst. 12, Q11Z33. http://dx.doi.org/10.1029/2011GC003810.

Sagnotti, L., Macrì, P., Lucchi, R.G., 2016. Geomagnetic paleosecular variation around 15 ka ago from NW Barents Sea cores (south of Svalbard). Geophys. J. Int. 204, 785–797. http://dx.doi.org/10.1093/gji/ggv485.

Snowball, I., Torii, M., 1999. Incidence and significance of magnetic iron sulphides in Quaternary sediments and soils. In: Maher, B.A., Thompson, R. (Eds.), Quaternary Climates, Environments, and Magnetism. Cambridge University Press, Cambridge, U.K., pp. 199–231.

Snowball, I., Zillén, L., Ojala, A., Saarinen, T., Sandgren, P., 2007. FENNOSTACK and FENNORPIS: varve dated Holocene paleomagnetic secular variation and relative palaeointensity stacks for Fennoscandia. Earth Planet. Sci. Lett. 255, 106–116. http://dx.doi.org/10.1016/j.epsl.2006.12.009.

Stoner, J.S., Andrews, J.T., 1999. The North Atlantic as a Quaternary magnetic archive. In: Maher, B., Thompson, R. (Eds.), Quaternary Climates, Environments and Magnetism. Cambridge University Press, Cambridge, pp. 49–80.

Stoner, J., Channel, J.E.T., Mazaud, A., Strano, S.E., Xuan, C., 2013. The influence of high-latitude flux lobes on the Holocene paleomagnetic record of IODP site U1305 and the northern North Atlantic. Geochem. Geophys. Geosyst. 14, 4623–4646. http://dx.doi.org/10.1002/ggge.20272.

Stuiver, M., Reimer, P.J., 1993. Extended 14C data base and revised CALIB 3.0 14C age calibration program. Radiocarbon 35, 215–230. http://dx.doi.org/10.1017/S0033822200013904.

Tauxe, L., 1993. Sedimentary records of relative paleointensity of the geomagnetic field: theory and practice. Rev. Geophys. 31, 319–354. http://dx.doi.org/10.1029/93RG01771.

Telford, R.J., Heegaard, E., Birks, H.J., 2004. The intercept is a poor estimate of a calibrated radiocarbon age. The Holocene 14, 296–298.

Thompson, R., Berglund, B., 1976. Late Weichselian geomagnetic 'reversal' as a possible example of the reinforcement syndrome. Nat. Publ. Group 263 (5577), 490–491.

Thompson, R., Turner, G.M., Stiller, M., Kaufman, A., 1985. Near east paleomagnetic secular variation recorded in sediments from the Sea of Galilee (Lake Kinneret). Quat. Res. 23, 175–188. http://dx.doi.org/10.1016/0033-5894(85)90027-4.

Thomsen, C., Blaume, F., Fohrmann, H., Peeken, I., Zeller, U., 2001. Particle transport processes at slope environments event driven flux across the Barents Sea continental margin. Mar. Geol. 175, 237–250. http://dx.doi.org/10.1016/S0025-3227(01)00143-8.

Thomson, J., Croudace, I.W., Rothwell, R.G., 2006. A geochemical application of the ITRAX scanner to a sediment core containing eastern Mediterranean sapropel units. In: Rothwell, R.G. (Ed.), New Techniques in Sediment Core Analysis. Geol. Soc. London Spec. Publ. Vol. 267. pp. 65–77. http://dx.doi.org/10.1144/GSL.SP.2006.267.01.05.

Turner, G.M., Thompson, R., 1981. Lake sediment record of the geomagnetic secular variation in Britain during Holocene times. Geophys. J. 65, 703–725. http://dx.doi.org/10.1111/j.1365-246X.1981.tb04879.x.

Turner, G.M., Thompson, R., 1982. Detransformation of the British geomagnetic secular variation record for Holocene times. Geophys. J. 70, 789–792. http://dx.doi.org/10.1111/j.1365-246X.1982.tb05983.x.

Vorren, T.O., Laberg, J.S., 1997. Trough mouth fans–palaeoclimate and ice-sheet monitors. Quat. Sci. Rev. 16, 865–881. http://dx.doi.org/10.1016/S0277-3791(97)00003-6.

Vorren, T.O., Lebesbye, E., Andreassen, K., Larsen, K.B., 1989. Glacigenic sediments on a passive continental margin an exemplified by the Barents Sea. Mar. Geol. 85, 251–272. http://dx.doi.org/10.1016/0025-3227(89)90156-4.

Vorren, T.O., Laberg, J.S., Blaume, F., Dowdeswell, J.A., Kenyon, N.H., Mienert, J., Rumohr, J., Werner, F., 1998. The Norwegian–Greenland sea continental margins: morphology and late quaternary sedimentary processes and environment. Quat. Sci. Rev. 17, 273–302. http://dx.doi.org/10.1016/S0277-3791(97)00072-3.

Wang, M., Zheng, H., Xie, X., Fan, D., Yang, S., Zhoa, Q., Wang, K., 2011. A 600-year flood history in the Yangtze River drainage: comparison between a subaqueous delta and historical records. Chin. Sci. Bull. 56, 188–195.

Zecchin, M., Rebesco, M., Lucchi, R.G., Caffau, M., Lantzsch, H., Hanebuth, T.J.J., 2016. Buried iceberg-keel scouring on the southern Spitsbergenbanken, NW Barents Sea. Mar. Geol. 382, 68–79. http://dx.doi.org/10.1016/j.margeo.2016.10.005.

Zolitschka, B., Negendank, J.F.W., 1996. Sedimentology, dating and palaeoclimatic interpretation of a 76.3 ka record from Lago Grande di Monticchio, southern Italy. Quat. Sci. Rev. 15, 101–112. http://dx.doi.org/10.1016/0277-3791(95)00022-4.